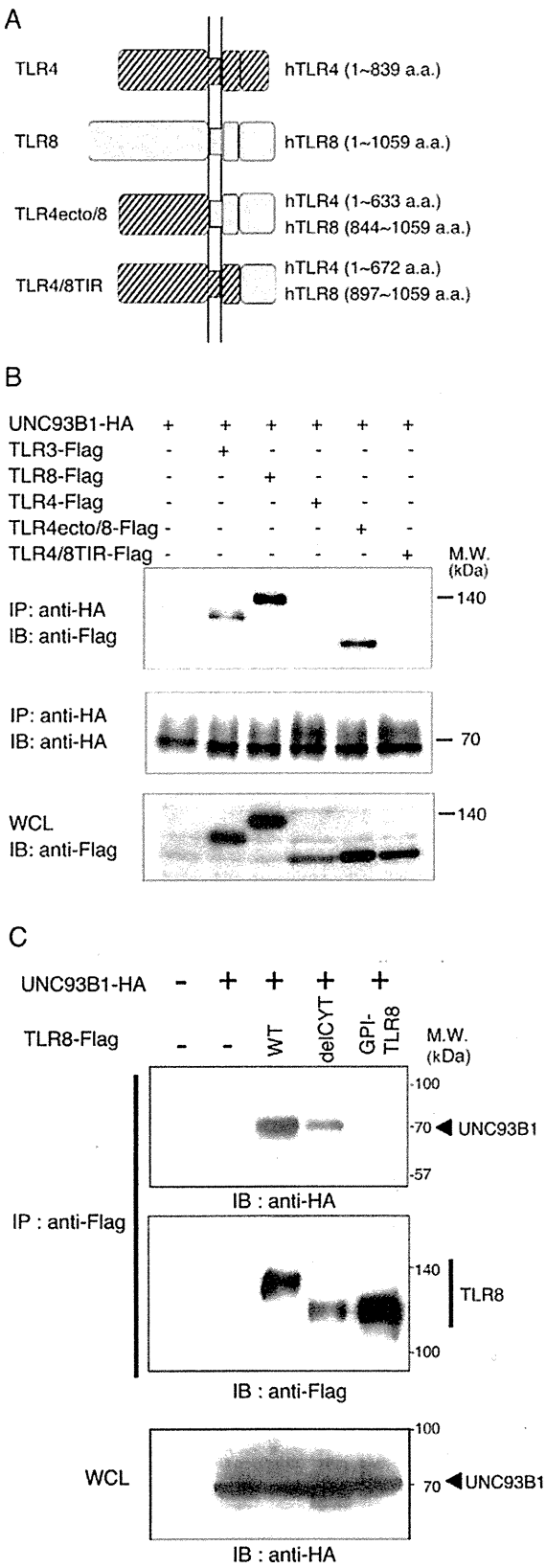

Figure 3. UNC93B1 physically associates with TLR8 through the transmembrane domain in HEK293FT cells. *A*, Schematic diagram of the TLR4/8 chimeric receptor constructs. *B*, *C*, HEK293FT cells were transfected with the corresponding vectors for expression of the indicated proteins. Twenty-four hours after transfection, cells were lysed in lysis buffer. The lysates were immunoprecipitated (IP) with anti-HA pAb (*B*) or anti-FLAG pAb (*C*), resolved using SDS-PAGE, and detected using immunoblotting (IB) with anti-FLAG M2 mAb or anti-HA mAb. Whole cell lysates (WCL) were subjected to immunoblotting with anti-FLAG mAb (*B*) or anti-HA mAb (*C*) to detect protein expression. Molecular weight markers are shown on the right.
doi:10.1371/journal.pone.0028500.g003

molecule interacts with the TIR domain of TLR8 and facilitates its trafficking to the early endosomes. As the BB loop in the TLR-TIR domain is critical for interaction with adaptor proteins, another region of the TLR8-TIR domain may participate in the association with the protein(s) regulating the receptor trafficking and intracellular localization of TLR8.

In humans, TLR7 and TLR8 recognize sequence-specific ssRNA and imidazoquinoline compounds in distinct cells and organelles, resulting in the induction of different immune responses via the same adaptor protein, MyD88. TLR7 ligands induce IFN-α production by plasmacytoid DCs, while TLR8 ligands induce proinflammatory cytokine production (e.g., TNF-α and IL-6) by myeloid DCs and monocytes [13]. This implies that TLR7 and TLR8 play distinct roles in the anti-viral immune response. Myeloid DCs express the viral RNA sensors, TLR3 and TLR8, on the endosomal membrane where they recognize virus-derived dsRNA and ssRNA, respectively. Activation of TLR3 by dsRNA results in the production of T helper 1 cytokines, such as IFN-α/β and interleukin (IL)-12p70, as well as DC maturation leading to the activation of cytotoxic T lymphocytes and natural killer (NK) cells [33]. TLR3 activation also induces TICAM-1-dependent gene expression in myeloid DCs, which mediates DC–NK reciprocal activation through cell–cell contact independently of type I IFN and IL-12 [34], whereas the key role of TLR8-mediated myeloid DC activation remains poorly understood. Detailed analyses of TLR8-mediated signaling in different cell types may give us new insight into the function of TLR8 in the anti-viral response.

Materials and Methods

Cell culture and reagents

HEK293 cells were maintained in Dulbecco's Modified Eagle's medium low glucose (Invitrogen) supplemented with 10% heat-inactivated FCS (BioSource Intl., Inc.) and antibiotics. HEK293FT cells were maintained in Dulbecco's Modified Eagle's medium high glucose supplemented with 0.1 mM NEAA, 10% heat-inactivated FCS and antibiotics. HeLa cells were maintained in Eagle's MEM (Nissui, Tokyo, Japan) supplemented with 1% L-glutamine and 10% heat-inactivated FCS. Human monocytes were isolated from peripheral blood mononuclear cells obtained from healthy individuals with a magnetic cell sorting system using anti-CD14-coated microbeads (Miltenyi Biotec, Gladbach, Germany). Anti-FLAG M2 monoclonal antibody (mAb), anti-HA polyclonal Ab (pAb), 4′,6-diamidine-2′-phenylindole dihydrochloride (DAPI), TRITC-labeled anti-phalloidin Ab, and saponin were purchased from Sigma-Aldrich. In addition, the following antibodies were used in this study: Alexa Fluor-conjugated secondary antibodies (Invitrogen), anti-HA mAb (Covance), anti-early endosome antigen 1 (EEA1) pAb (Affinity Bioreagents), anti-calnexin pAb and anti-calreticulin pAb (Stressgen, Victoria, Canada), anti-p115 pAb (Calbiochem, Darmstadt, Germany),

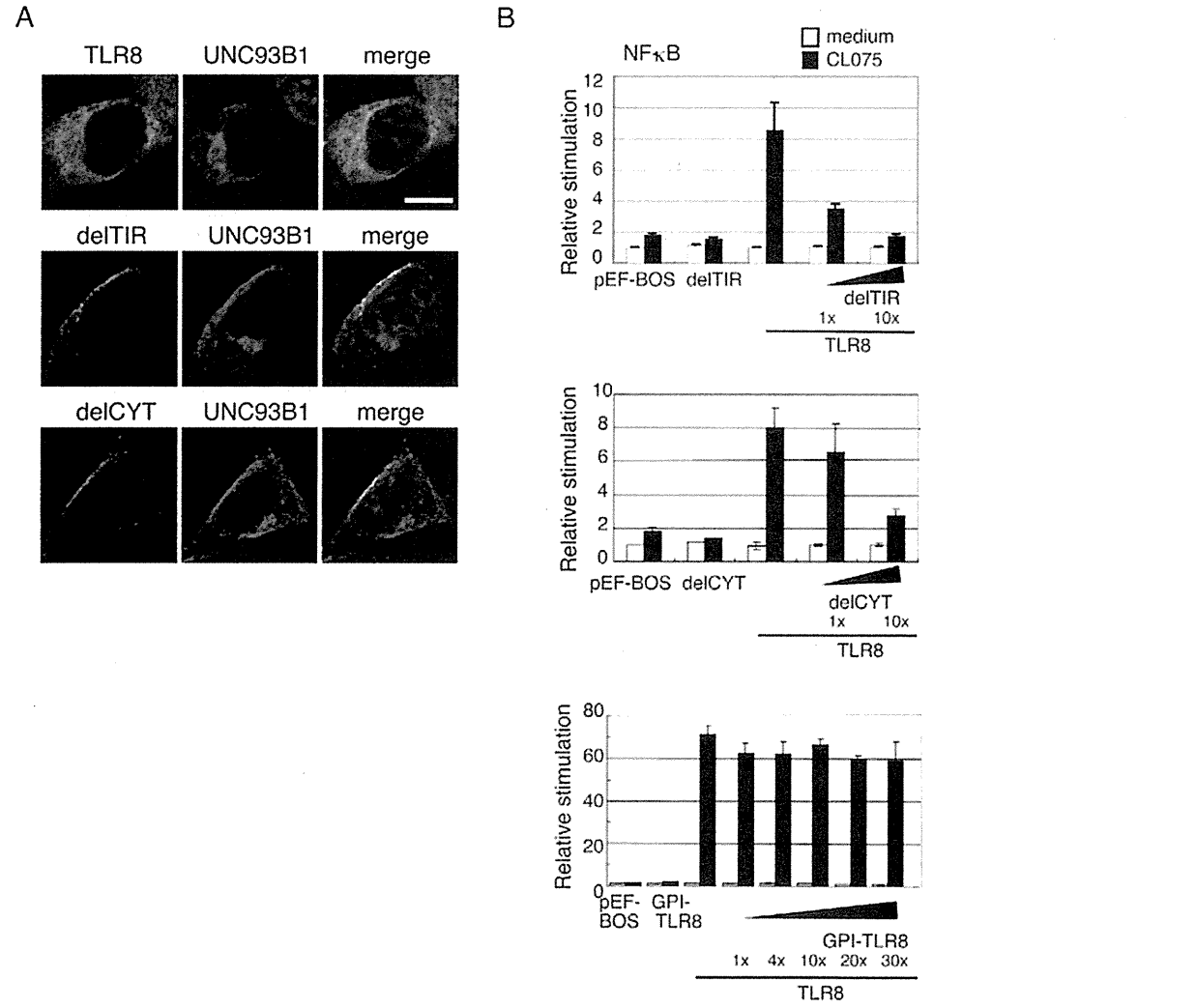

Figure 4. UNC93B1 colocalizes with surface-expressed TLR8 mutants. *A*, HeLa cells transiently expressing wild-type TLR8, delCYT, or delTIR were incubated with anti-FLAG mAb and anti-human UNC93B1 pAb followed by an Alexa Fluor 568-conjugated anti-mouse IgG and Alexa Fluor 488-conjugated anti-rabbit IgG. Representative confocal images are shown. Green, endogenous UNC93B1; red, TLR8; blue, nuclei stained with DAPI. Scale bar:10 μm. *B*, Surface-expressed TLR8 mutant proteins inhibited CL075-induced TLR8-mediated NF-κB activation. Luciferase activity of HEK293 cells transfected with the ELAM-promoter-luciferase reporter and expression plasmid for wild-type TLR8 together with increasing amounts of plasmid expressing delTIR (upper graph), delCYT (middle graph), or GPI-TLR8 (lower graph). Twenty-four hours after transfection, the cells were stimulated with 2.5 μg/mL of CL075 or left untreated. After 24 hours, the luciferase reporter activities were measured and expressed as the fold induction relative to the activity of unstimulated cells. Representative data from a minimum of three separate experiments are shown (mean and s.d. of triplicate assays).
doi:10.1371/journal.pone.0028500.g004

anti-LAMP-1 mAb (Biolegend), anti-MPR pAb (Abcam, Cambridge, UK), anti-human TLR8 mAb (Dendritics, LYON, France) and anti-human UNC93B1 pAb (ProSci Inc., Poway, CA). Lysotracker was from Invitrogen. CL075 was from InvivoGen.

Plasmids

Complementary DNAs for human TLR3 and TLR8 were cloned in our laboratory by RT-PCR from the mRNA of monocyte-derived immature DCs and were ligated into the cloning site of the expression vector, pEF-BOS, which was provided by Dr. S. Nagata (Kyoto University). The FLAG-tag or HA-tag was inserted into the C-terminal of pEF-BOS expression vectors for hTLR3 or hTLR8. The truncated TLR8 mutants, delTIR (1-896 a.a.) and delCYT (1-866 a.a.) were generated by PCR with Pfu Turbo DNA polymerase (STRATAGENE) using specific primers (forward primer; 5′-GACTACAAAGACGATGACGACAAGTAAGCG-3′, reverse primer for delTIR; 5′-GAAAGTTTGCGATGTGGAAAGAGACCTGTA-3′, reverse primer for delCYT; 5′-AGCCAGGGCAGCCAACATAACCATGGTGGT-3′) as described [21]. GPI-hTLR8 was constructed in the pEF-BOS expression vector by ligation of PCR products corresponding to the TLR8 ectodomain (45-843 a.a.) sequentially attached with the preprotrypsin signal sequence, HAT, and Flag at the N-terminus, and the GPI-attachment sequence from CD55 at

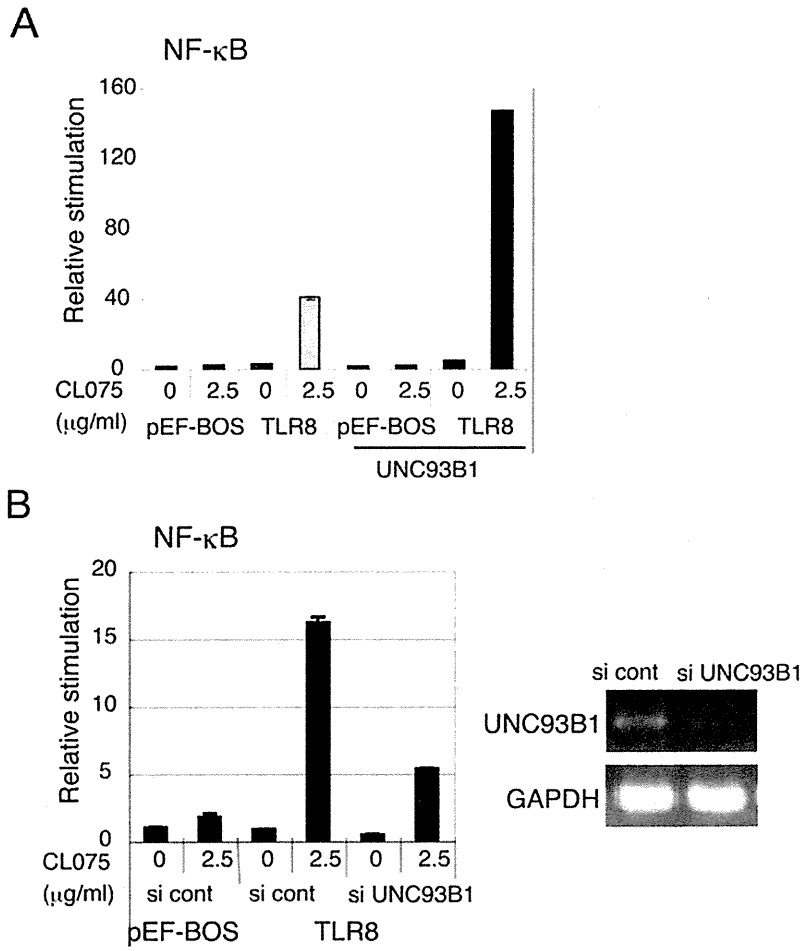

Figure 5. UNC93B1 is indispensable for TLR8-mediated signaling. *A*, Upregulation of TLR8-mediated NF-κB activation by co-expression with UNC93B. HEK293 cells were transfected with the indicated plasmid together with the ELAM reporter plasmid. Twenty-four hours after transfection, the cells were stimulated with CL075 or left untreated. After 6 hours, the luciferase reporter activities were measured and expressed as the fold induction relative to the activity of unstimulated cells. Representative data from three separate experiments are shown. *B*, TLR8-mediated NF-κB activation is downregulated by knockdown of UNC93B1. UNC93B1 siRNA or negative control siRNA was transfected into HEK293 cells together with the reporter plasmids and TLR8 expression plasmid. Forty-eight hours after transfection, cells were stimulated with CL075 for 6 hours and the luciferase reporter activities were measured. Data are representative of three independent experiments (mean and s.d. of triplicate assays). The expression of endogenous UNC93B1 and GAPDH mRNAs were examined using RT-PCR 48 hours after siRNA transfection (right panels).
doi:10.1371/journal.pone.0028500.g005

the C-terminus. The TLR4/TLR8 chimeric receptor, TLR4ecto/8, was constructed in the expression vector pEF-BOS by ligation of PCR products corresponding to amino acids 1-633 of human TLR4 ectodomain and amino acids 844-1059 of human TLR8. Another TLR4/TLR8 chimeric receptor, TLR4/8TIR, was constructed by the ligation of PCR products corresponding to amino acids 1-672 of human TLR4 (ectodomain, TM, and linker region) and amino acids 897-1059 of the human TLR8 TIR domain. Both constructs were FLAG tagged at the C-terminus. A plasmid for human UNC93B1 (pMD2/UNC93B1) and the expression plasmid for TLR4 (pEF-BOS/TLR4) were provided by Dr. K. Miyake (The University of Tokyo). The HA-tag was inserted into the C-terminal of the pEF-BOS expression vector for human UNC93B1. The human UNC93B1 mutant, hUNC93B1(H412R), in which the arginine residue at position 412 was substituted for a histidine residue, was made by site-directed mutagenesis.

Confocal microscopy

HeLa cells (1.0×10^5 cells/well) were plated onto micro cover glasses (Matsunami, Tokyo, Japan) in a 24-well plate. The following day, cells were transfected with the indicated plasmids using Fugene HD (Roche Diagnostics) or Lipofectamine 2000 (Invitrogen). Twenty-four hours after transfection, cells were fixed with 3% formalin for 30 min and permeabilized with PBS containing 0.5% saponin and 1% BSA for 30 min or fixed with 4% paraformaldehyde for 30 min and permeabilized with PBS containing 0.2% Triton X-100 and 1% BSA for 15 min (for staining of endogenous UNC93B1). In the case of monocytes, cells were fixed with 4% paraformaldehyde for 15 min. For the staining of late endosome, cells were permeabilized with PBS containing 100 μg/ml of digitonin and 1% BSA for 30 minutes. Fixed cells were blocked in PBS containing 1% BSA, and were then labeled with the indicated primary Abs (2~10 μg/ml) for 60 min at room temperature. Alexa-conjugated secondary Abs (1:400) were used

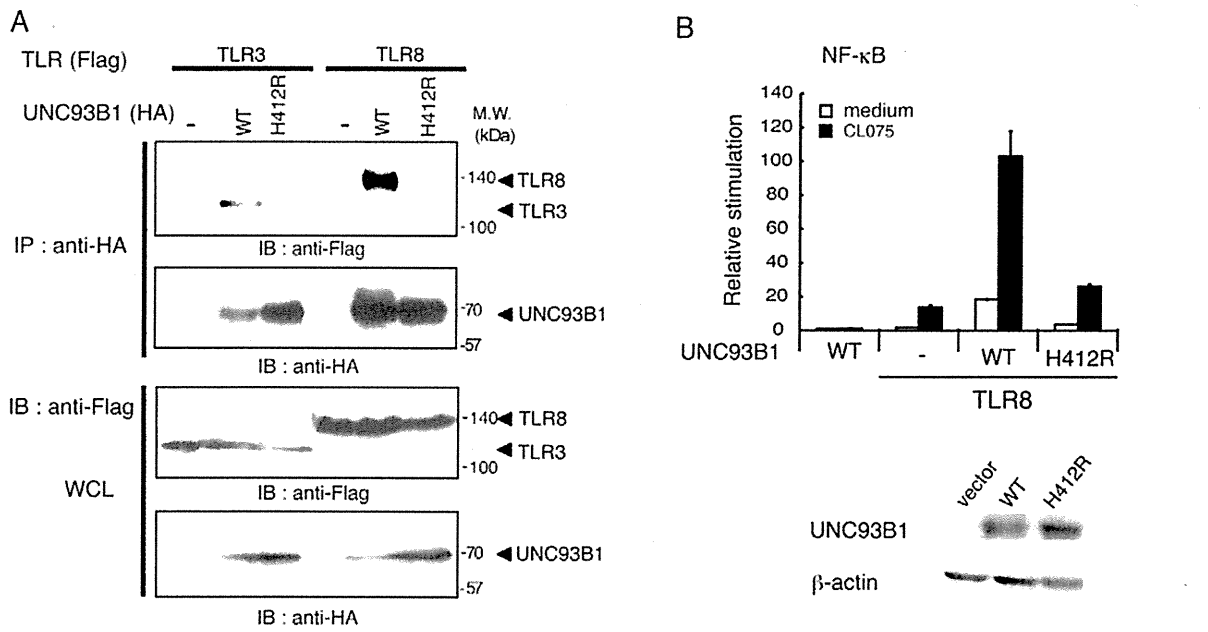

Figure 6. His412 is essential for the interaction of UNC93B1 with TLR8 and TLR8-mediated signaling. *A*, HEK293FT cells were transfected with the corresponding vectors for expression of the indicated proteins. The cell lysates were immunoprecipitated (IP) with anti-HA pAb, resolved by SDS-PAGE and detected by immunoblotting (IB) with anti-FLAG M2 or anti-HA mAb. Whole cell lysates (WCL) were subjected to immunoblotting with anti-FLAG or anti-HA mAb to detect protein expression. Molecular weight markers are shown on the right. *B*, HEK293 cells were transfected with the indicated plasmid together with the ELAM reporter plasmid. Cells were stimulated with CL075 or left untreated and the luciferase reporter activities were measured. Representative data from three separate experiments are shown. *Lower panels*, protein expression of wild-type and mutant UNC93B1 in HEK293 cells. β-actin blots are shown as loading controls.
doi:10.1371/journal.pone.0028500.g006

to visualize the staining of the primary Abs. After mounting with ProLong Gold with DAPI (Molecular Probes), cells were visualized at a magnification of ×63 with an LSM510 META microscope (Zeiss, Jena, Germany).

Reporter assay

HEK293 cells (5×10^5 cells/well) cultured in 24-well plates were transfected with the indicated plasmid together with the reporter plasmid and an internal control vector, phRL-TK (Promega), using FuGENE HD. The reporter plasmid containing the ELAM-1 promoter was constructed in our laboratory. Twenty-four hours after transfection, cells were stimulated with 2.5 μg/mL CL075. The cells were collected 6 hours after stimulation and then lysed. The *Firefly* and *Renilla* luciferase activities were determined using a dual-luciferase reporter assay kit (Promega). The *Firefly* luciferase activity was normalized with the *Renilla* luciferase activity and was expressed as the fold induction relative to the activity in unstimulated vector-transfected cells. All assays were performed in triplicate.

RNAi

siRNA duplexes (UNC93B1:ID #s37730, negative control: catalog #AM4635) were obtained from Ambion-Applied Biosystems. HEK293 cells cultured in 24-well plates were transfected with 20 pmol of each siRNA together with the expression vector for hTLR8 (40 ng), ELAM reporter plasmid (60 ng), an internal control vector (1.5 ng) and empty vector (400 ng) using Lipofectamin 2000. Forty-eight hours after transfection, cells were washed once and then stimulated with 2.5 μg/ml CL075 for 6 hours. Knockdown of UNC93B1 was confirmed 48 hours after siRNA transfection by RT-PCR using specific primers (UNC93B1: forward primer 5′-GCCCATGATTTATTTCCTGAACCACTACC-3′ and reverse primer, 5′-GTGTGCTGAGTCCAGTCTTGTTCAG-3′, GAPDH: forward primer 5′-GAGTCAACGGATTTGGTCGT-3′ and reverse primer 5′- TTGATTTTGGAGGGATCTCG-3′). Experiments were repeated three times for confirmation of the results.

Immunoprecipitation

HEK293FT cells (2.5×10^5 cells/well) cultured in 12-well plates were transfected with the indicated plasmids using Lipofectamine 2000 (Invitrogen). After 24 hours, cells were washed twice with DPBS. Washed cells were lysed in 1% digitonin lysis buffer (50 mM Tris-HCl (pH 7.4), 150 mM NaCl, 5 mM EDTA, 2 mM PMSF, and a protease inhibitor cocktail) or 1% NP-40 lysis-washing buffer (50 mM Tris-HCl (pH 7.4), 150 mM NaCl, 10 mM EDTA, 1 mM PMSF, and a protease inhibitor cocktail) in Fig. 2. Lysates were clarified by centrifugation, pre-cleared with Protein G-Sepharose (GE Healthcare, Buckinghamshire, UK), and incubated with anti-FLAG mAb or anti-HA pAb. The immunoprecipitates were recovered by incubation with Protein G-Sepharose, washed three times with 0.1% digitonin washing buffer (50 mM Tris-HCl (pH 7.4), 150 mM NaCl, 5 mM EDTA, 1 mM PMSF) or 1% NP-40 lysis-washing buffer and then resuspended in denaturing buffer. Samples were analyzed by SDS-PAGE under reducing conditions followed by immunoblotting with anti-tag Abs.

Supporting Information

Figure S1 Flow cytometric analysis of cell surface expression of GPI-hTLR8 transiently expressed in HeLa cells. HeLa cells were

transfected with the empty vector or the expression plasmid for FLAG-tagged GPI-hTLR8 using Lipofectamine 2000 in 12-well plates. Twenty-four hours after transfection, cells were washed and incubated with anti-FLAG M2 mAb or mouse IgG1 in the presence of human IgG for 30 min at 4° C in FACS buffer (DPBS containing 0.5% BSA and 0.1% sodium azide). Cells were washed twice in FACS buffer and incubated with FITC-labeled secondary antibody (American Qualex) for 30 min at 4° C. For intracellular staining, cells were permeabilized with permeabilizing solution (BD) for 10 min at room temperature, and then stained with anti-FLAG mAb in the presence of 10% goat serum and FITC-labeled secondary Ab. Cells were analyzed using a FACS Calibur (BD). Shaded histogram: control mouse IgG 1 staining; thick line: anti-FLAG mAb staining. Inset values indicate the mean fluorescent intensities specific for the anti-FLAG mAb.
(EPS)

Figure S2 Forced expression of TLR8 mutants affects the endosomal localization of wild-type TLR8. *A*, Confocal images show HeLa cells co-expressing HA-tagged wild-type TLR8 and FLAG-tagged TLR8 mutants. Cells were fixed and stained with anti-FLAG mAb and anti-HA pAb, followed by Alexa568-labeled goat anti-mouse Ab and Alexa488-labeled goat anti-rabbit Ab. TLR8 mutants delCYT and delTIR were anchored on plasma membrane and did not merge with wild-type TLR8. Red, TLR8 mutants; green, wild-type TLR8; blue, nuclei stained with DAPI; bar, 10 μm. *B*, Cells were transfected with FLAG-tagged wild-type TLR8 alone (upper panels), together with FLAG-tagged delCYT (middle panels) or FLAG-tagged delTIR (lower panels), and stained with anti-FLAG mAb and anti-EEA1 pAb, followed by Alexa568-labeled goat anti-mouse Ab and Alexa488-labeled goat anti-rabbit Ab. Wild-type TLR8 was expressed intracellularly and colocalized with EEA1 (upper panels). When delCYT or delTIR was expressed with wild-type TLR8, colocalization between TLR8 and EEA1 was decreased (middle and lower panels). Red, TLR8; green, early endosome marker EEA1; blue, nuclei stained with DAPI; bar, 10 μm.
(EPS)

Acknowledgments

We are grateful to Drs. H. Oshiumi, H. Shime, T. Ebihara, A. Matsuo, H. H. Aly, H. Takaki, and J. Kasamatsu for invaluable discussions. Thanks are also due to Dr. K. Miyake (University of Tokyo, Tokyo) for providing plasmids.

Author Contributions

Conceived and designed the experiments: HI KF TS MM. Performed the experiments: HI MT AW KI. Analyzed the data: MT TS MM. Wrote the paper: MM.

References

1. Medzhitov R, Janeway CA, Jr. (1997) Innate immunity: the virtues of a nonclonal system of recognition. Cell 91: 295–298.
2. Akira S, Uematsu S, Takeuchi O (2006) Pathogen recognition and innate immunity. Cell 124: 783–801.
3. Kono H, Rock KL (2008) How dying cells alert the immune system to danger. Nat Rev Immunol 8: 279–289.
4. Medzhitov R, Preston-Hurlburt P, Janeway CA, Jr. (1997) A human homologue of the Drosophila Toll protein signals activation of adaptive immunity. Nature 388: 394–397.
5. Muzio M, Bosisio D, Polentarutti N, D'amico G, Stoppacciaro A, et al. (2000) Differential expression and regulation of toll-like receptors (TLR) in human leukocytes: selective expression of TLR3 in dendritic cells. J Immunol 164: 5998–6004.
6. Kadowaki M, Ho S, Antonenko S, de Waal Malefyt R, Kastelein RA, et al. (2001) Subsets of human dendritic cell precursors express different Toll-like receptors and respond to different microbial antigens. J Exp Med 194: 863–870.
7. Hornung V, Rothenfusser S, Britsch S, Krug A, Jahrsdorfer B, et al. (2002) Quantitative expression of Toll-like receptor 1-10 mRNA in cellular subsets of human peripheral blood mononuclear cells and sensitivity to CpG oligodeoxynucleotides. J Immunol 168: 4531–4537.
8. Matsumoto M, Funami K, Tanabe M, Oshiumi H, Shingai M, et al. (2003) Subcellular localization of Toll-like receptor 3 in human dendritic cells. J Immunol 171: 3154–3162.
9. Chuang T-H, Ulevitch RJ (2000) Cloning and characterization of a sub-family of human Toll-like receptors: hTLR7, hTLR8 and hTLR9. Eur Cytokine Netw 11: 372–378.
10. Du X, Poltorak A, Wei Y, Beutler B (2000) Three novel mammalian toll-like receptors: gene structure, expression, and evolution. Eur Cytokine Netw 11: 362–371.
11. Heil F, Hemmi H, Hochrein H, Ampenberger F, Kirschning C, et al. (2004) Species-specific recognition of single-stranded RNA via toll-like receptor 7 and 8. Science 303: 1526–1529.
12. Diebold SS, Kaisho T, Hemmi H, Akira S, Sousa RC (2004) Innate antivial responses by means of TLR7-mediated recognition of single-stranded RNA. Science 303: 1529–1531.
13. Gorden KB, Gorski KS, Gibson SJ, Kedl RM, Kieper WC, et al. (2005) Synthetic TLR agonists reveal functional differences between human TLR7 and TLR8. J Immunol 174: 1259–1268.
14. Jurk M, Heil F, Vollmer J, Schetter C, Krieg AM, et al. (2002) Human TLR7 or TLR8 independently confer responsiveness to the antiviral compound R-848. Nat Immunol 3: 499.
15. Ma Y, Li J, Chiu I, Wang Y, Sloane JA, et al. (2006) Toll-like receptor 8 functions as a negative regulator of neurite outgrowth and inducer of neuronal apoptosis. J Cell Biol 28: 209–215.
16. Peng G, Guo Z, Kiniwa Y, Voo KS, Peng W Fu, et al. (2005) Toll-like receptor 8-mediated reversal of CD4+ regulatory T cell function. Science 309: 1380–1384.
17. Jongbloed SL, Kassianos AJ, McDonald KJ, Clark GJ, Ju X, et al. (2010) Human CD141+ (BDCA-3+) dendritic cells (DCs) represent a unique myeloid DC subset that cross-presents necrotic cell antigens. J Exp Med 207: 1247–1260.
18. Oshiumi H, Matsumoto M, Funami K, Akazawa T, Seya T (2003) TICAM-1, an adaptor molecule that participates in Toll-like receptor 3-mediated interferon-beta induction. Nat Immunol 4: 161–167.
19. Yamamoto M, Sato S, Hemmi H, Hoshino K, Kaisho T, et al. (2003) Role of adaptor TRIF in the MyD88-independent Toll-like receptor signaling pathway. Science 301: 640–643.
20. Funami K, Sasai M, Ohba Y, Oshiumi H, Seya T, et al. (2007) Spatiotemporal mobilization of Toll/IL-1 receptor domain-containing adaptor molecule-1 in response to dsRNA. J Immunol 179: 6867–6872.
21. Funami K, Matsumoto M, Oshiumi H, Akazawa T, Yamamoto A, et al. (2004) The cytoplasmic 'linker region' in Toll-like receptor 3 controls localization and signaling. Int Immunol 16: 1143–1154.
22. Nishiya T, DeFranco AL (2004) Ligand-regulated chimeric receptor approach reveals distinctive subcellular localization and signaling properties of the Toll-like receptors. J Biol Chem 279: 19008–19017.
23. Barton GM, Kagan JC, Medzhitov R (2006) Intracellular localization of Toll-like receptor 9 prevents recognition of self DNA but facilitates access to viral DNA. Nat Immunol 7: 49–56.
24. Brinkmann MM, Spooner E, Hoebe K, Beutler B, Ploegh HL, et al. (2007) The interaction between the ER membrane protein UNC93B and TLR3, 7, and 9 is crucial for TLR signaling. J Cell Biol 177: 265–275.
25. Kim Y-M, Brinkmann MM, Paquet M-E, Ploegh HL (2008) UNC93B1 delivers nucleotide-sensing toll-like receptors to endolysosomes. Nature 452: 234–238.
26. Ewald SE, Lee BL, Lau L, Wickliffe KE, Shi G-P, et al. (2008) The ectodomain of Toll-like receptor 9 is cleaved to generate a functional receptor. Nature 456: 658–662.
27. Park B, Brinkmann MM, Spooner E, Lee CC, Kim YM, et al. (2008) Proteolytic cleavage in an endolysosomal compartment is required for activation of Toll-like receptor 9. Nat Immunol 9: 1407–141.
28. Fukui R, Saitoh S, Matsumoto F, Kozuka-Hara H, Oyama M, et al. (2009) Unc93B1 biases Toll-like receptor responses to nucleic acid in dendritic cells toward DNA- but against RNA-sensing. J Exp Med 206: 1339–1350.
29. Tabeta K, Hoebe K, Janssen EM, Du X, Georgel P, et al. (2006) The Unc93B1 mutation 3d disrupts exogeneous antigen presentation and signaling via Toll-like receptors 3, 7 and 9. Nat Immunol 7: 146–164.
30. Gibbard RJ, Morley, PJ, Gay NJ (2006) Conserved features in the extracellular domain of human Toll-like receptor 8 are essential for pH-dependent signaling. J Biol Chem 281: 27503–27511.
31. Leifer CA, Brooks JC, Hoelzer K, Lopez J, Kennedy MN, et al. (2006) Cytoplasmic Targeting motifs control localization of Toll-like receptor 9. J Biol Chem 281: 35585–35592.
32. Zhua J, van Drunen Littel-van den Hurka S, Brownliea R, Babiuka LA, Pottera A, et al. (2009) Multiple molecular regions confer intracellular localization of bovine Toll-like receptor 8. Molec Immunol 46: 884–892.

33. Matsumoto M, Seya T (2008) TLR3: Interferon induction by double-stranded RNA including poly(I:C). Adv Drug Del Rev 60: 805–812.

34. Ebihara T, Azuma M, Oshiumi H, Kasamatsu J, Iwabuchi K, et al. (2010) Identification of a polyI:C-inducible membrane protein that participates in dendritic cell-mediated natural killer cell activation. J Exp Med 207: 2675–2687.

OPEN ACCESS Freely available online

PLoS one

Phosphoinositide 3-Kinaseγ Controls the Intracellular Localization of CpG to Limit DNA-PKcs-Dependent IL-10 Production in Macrophages

Kaoru Hazeki[1]*, Yukiko Kametani[1], Hiroki Murakami[1], Masami Uehara[1], Yuki Ishikawa[1], Kiyomi Nigorikawa[1], Shunsuke Takasuga[2], Takehiko Sasaki[2], Tsukasa Seya[3], Misako Matsumoto[3], Osamu Hazeki[1]

1 Division of Molecular Medical Science, Graduate School of Biomedical Sciences, Hiroshima University, Hiroshima, Japan, **2** Department of Pathology and Immunology, Akita University School of Medicine, Akita, Japan, **3** Department of Microbiology and Immunology, Hokkaido University Graduate School of Medicine, Sapporo, Japan

Abstract

Synthetic oligodeoxynucleotides containing unmethylated CpG motifs (CpG) stimulate innate immune responses. Phosphoinositide 3-kinase (PI3K) has been implicated in CpG-induced immune activation; however, its precise role has not yet been clarified. CpG-induced production of IL-10 was dramatically increased in macrophages deficient in PI3Kγ (p110$\gamma^{-/-}$). By contrast, LPS-induced production of IL-10 was unchanged in the cells. CpG-induced, but not LPS-induced, IL-10 production was almost completely abolished in SCID mice having mutations in DNA-dependent protein kinase catalytic subunit (DNA-PKcs). Furthermore, wortmannin, an inhibitor of DNA-PKcs, completely inhibited CpG-induced IL-10 production, both in wild type and p110$\gamma^{-/-}$ cells. Microscopic analyses revealed that CpG preferentially localized with DNA-PKcs in p110$\gamma^{-/-}$ cells than in wild type cells. In addition, CpG was preferentially co-localized with the acidic lysosomal marker, LysoTracker, in p110$\gamma^{-/-}$ cells, and with an early endosome marker, EEA1, in wild type cells. Over-expression of p110γ in Cos7 cells resulted in decreased acidification of CpG containing endosome. A similar effect was reproduced using kinase-dead mutants, but not with a ras-binding site mutant, of p110γ. Thus, it is likely that p110γ, in a manner independent of its kinase activity, inhibits the acidification of CpG-containing endosomes. It is considered that increased acidification of CpG-containing endosomes in p110$\gamma^{-/-}$ cells enforces endosomal escape of CpG, which results in increased association of CpG with DNA-PKcs to up-regulate IL-10 production in macrophages.

Citation: Hazeki K, Kametani Y, Murakami H, Uehara M, Ishikawa Y, et al. (2011) Phosphoinositide 3-Kinaseγ Controls the Intracellular Localization of CpG to Limit DNA-PKcs-Dependent IL-10 Production in Macrophages. PLoS ONE 6(10): e26836. doi:10.1371/journal.pone.0026836

Editor: Jianming Qiu, University of Kansas Medical Center, United States of America

Received July 7, 2011; **Accepted** October 4, 2011; **Published** October 28, 2011

Funding: This work was supported by Grant-in-Aid for Scientific Research (C), KAKENHI20590060, 22590065 and 23590078, and Grant-in-Aid for Scientific Research on Innovative Areas, KAKENHI22114008. The funders had no role in study design, data collection and analysis, decision to publish, or preparation of the manuscript.

Competing Interests: The authors have declared that no competing interests exist.

* E-mail: khazeki@hiroshima-u.ac.jp

Introduction

Oligodeoxynucleotides containing unmethylated CpG motifs (CpG) are powerful immune adjuvants that induce the production of cytokines, including IL-6, IL-10, IL-12, IFN-α/β, and TNF-α [1,2]. Although previous studies have established that CpG-induced immune responses are mediated by endosomal TLR9 [3–5], cytoplasmic DNA-PKcs are also involved in CpG-signaling independent of TLR9 [6,7]. Thus, intracellular trafficking of CpG is critical to select downstream signaling molecules, which determine the cytokine species produced by macrophages [7,8].

Phosphoinositide 3-kinase (PI3K) has been reported to be both a positive and negative regulator of CpG-mediated cytokine production. CpG-induced IL-12 production is increased in plasmacytoid dendritic cells (pDC) from p85$\alpha^{-/-}$ mice, and by treatment of wild-type pDC with wortmannin [9]. Likewise, CpG-induced iNOS expression is increased by treating RAW264.7 cells with wortmannin [10]. By contrast, another group has reported that wortmannin inhibits CpG-induced production of IL-12, IL-6, TNF-α, and NO from RAW264.7 cells [11]. This inhibition has been considered to be the result of wortmannin-mediated disruption of class III PI3K signaling, which is responsible for CpG uptake [11]. Similarly, wortmannin inhibits CpG-induced IL-12 production by inhibiting CpG internalization in mouse-derived bone marrow cells [12]. In human pDC, another PI3K inhibitor, LY294002, also inhibits CpG-induced type I IFN production [13]. In this case, the uptake and endosomal trafficking of CpG are not affected, but nuclear translocation of IRF-7 was inhibited by LY294002, and also, by a specific inhibitor of PI3Kδ, IC87114 [13]. In addition, the PI3K/mTOR/p70S6K pathway plays a substantial role in the spatial interaction of TLR9/MyD88/IRF7, which is indispensable for the induction of type I IFN production by pDC [14]. These reports have indicated that PI3Ks play some roles in trafficking of CpG itself or its downstream molecules.

Pan- and/or some other specific PI3K inhibitors were used in all of the previous studies described above. All of these inhibitors bind competitively to the ATP binding pocket of PI3Ks and block kinase activity. Since DNA-dependent protein kinase catalytic

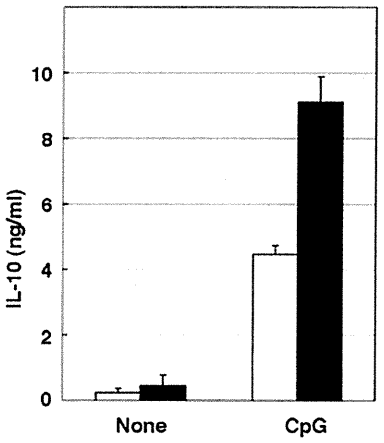

Figure 1. Increased IL-10 production following CpG stimulation of p110γ$^{-/-}$ cells. Macrophages from wild type (open bar) or p110γ$^{-/-}$ mice (solid bar) were incubated in 24-well plates with 10 ng/mL LPS, 200 ng/mL CpG, 50 μg/mL polyI:C or 200 nM Malp2 for 18 h. The amount of IL-10 in the medium was determined by ELISA. The values are the means ± SD of duplicate cultures from three independent experiments.
doi:10.1371/journal.pone.0026836.g001

subunit (DNA-PKcs) shares similar ATP binding site as a member of the PI3K-like kinase family, these inhibitors, even isoform-specific inhibitors, more or less inhibit DNA-PKcs [15]. This makes it difficult to elucidate the precise role of DNA-PKcs and PI3Ks in CpG-mediated cytokine production. In this paper, we used class IB PI3K (p110γ) knockout mice and SCID mice having mutations in DNA-PKcs to estimate their roles in CpG-mediated cytokine production. In agreement with a current report, DNA-PKcs play a substantial role in CpG-mediated IL-10 production in macrophages [7]. By contrast, p110γ specifically down-regulates IL-10 production following CpG-stimulation. Quantitative analysis of microscopic images showed that CpG localized preferentially with DNA-PKcs in the cytosol in p110γ$^{-/-}$ cells to a greater extent than in wild-type cells. We propose a novel regulatory role of p110γ in CpG-induced production of IL-10 through modulation of the intracellular trafficking of CpG.

Results

p110γ deficiency specifically increased IL-10 production upon CpG stimulation in macrophages

Mouse macrophages generated IL-10 in response to CpG (Fig. 1). Since PI3K has been implicated in the regulation of TLR-induced IL-10 production [16], we tested the effect of p110γ depletion on IL-10 production. CpG-induced IL-10 production was dramatically increased in macrophages from p110γ$^{-/-}$ mouse (Fig. 1). Although IL-10 production sometimes varied extremely between experiments, IL-10 production in wild type mice was always approximately half of that in p110γ$^{-/-}$ mice in each paired experiment. We also tested the cytokine production using macrophages from p85α$^{-/-}$ mice, and from p110δ$^{KD/KD}$ mice; neither displayed CpG-specific changes in IL-10 production similar to what was seen with p110γ$^{-/-}$ cells (data not shown).

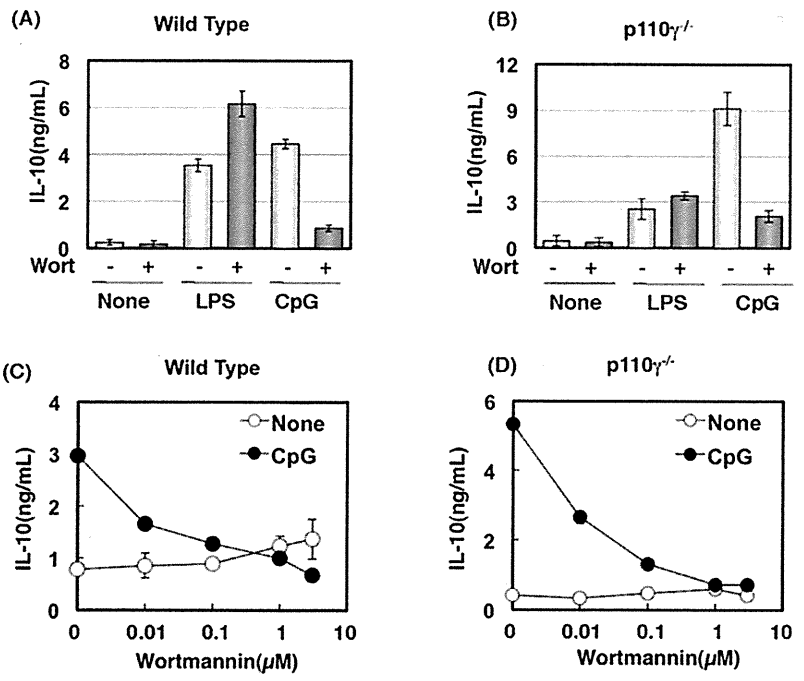

Figure 2. Inhibition of CpG-induced IL-10 production by wortmannin. Macrophages from wild type (A, C) or p110γ$^{-/-}$ mice (B, D) were pre-incubated with 0.1 μM (+ in A, B), or increasing concentration of wortmannin (C, D) for 15 min, followed by the addition of 10 ng/mL LPS (A, B) or 200 ng/mL CpG (A–D), for 18 h. The amount of IL-10 in the medium was determined by ELISA. The values are the means ± SD of duplicate cultures from three independent experiments.
doi:10.1371/journal.pone.0026836.g002

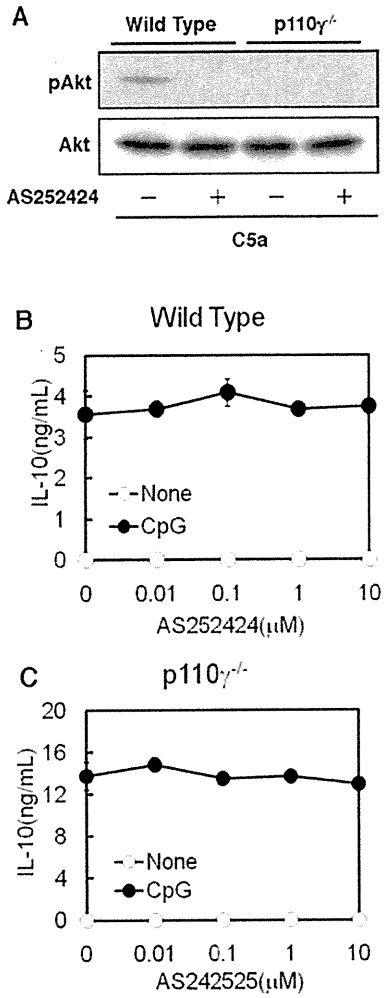

Figure 3. Irrelevance of the kinase activity of p110γ in the regulation of IL-10 production. (A) Macrophages from wild type or p110γ$^{-/-}$ mice were pre-incubated with 10 μM AS252424 for 15 min, followed by the addition of 100 ng/mL C5a for 5 min. Total cell lysates from the treated cells were analyzed by Western blot. (B and C) Macrophages from wild type (B) or p110γ$^{-/-}$ mice (C) were pre-incubated with increasing concentrations of AS252424 for 15 min, followed by the addition of 200 ng/mL CpG for 18 h. The amount of IL-10 in the medium was determined by ELISA. The values are the means ± SD of duplicate cultures from three independent experiments.
doi:10.1371/journal.pone.0026836.g003

Wortmannin inhibited IL-10 production induced by CpG, but increased that induced by LPS

Macrophages were treated with a pan-PI3K inhibitor, wortmannin. CpG-induced IL-10 production was almost completely inhibited by wortmannin while LPS-induced IL-10 production was rather increased in wild type cells (Fig. 2A). The effect of wortmannin on LPS-induced IL-10 production may be the result of the inhibition of p110γ, because the augmentation was not observed in p110γ$^{-/-}$ cells (Fig. 2B). However, wortmannin inhibited severely CpG-induced IL-10 production in p110γ$^{-/-}$ cells, as well as in wild type cells (Fig. 2C. D). The inhibition by wortmannin was specific to IL-10 production, because IL-12 production was unchanged by the treatment (data not shown).

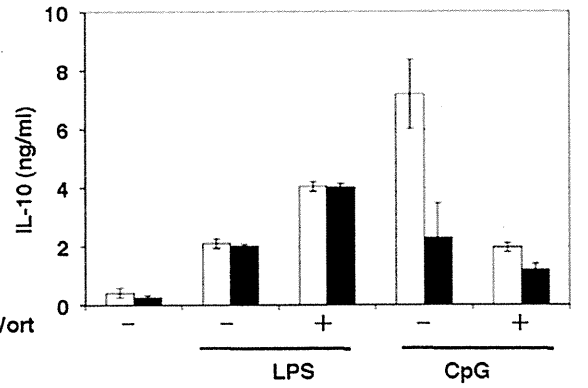

Figure 4. Failure of CpG to stimulate IL-10 production in SCID mice. Macrophages from wild type (open bar) or SCID (solid bar) mice were preincubated with 0.1 μM wortmannin (+) or vehicle (−) for 15 min, followed by the addition of 10 ng/mL LPS or 200 ng/mL CpG, for 18 h. The amount of IL-10 in the medium was determined by ELISA. The values are the means ± SD of duplicate cultures from three independent experiments.
doi:10.1371/journal.pone.0026836.g004

These data indicate that the target molecule of wortmannin responsible for the suppression of CpG-induced IL-10 was not p110γ.

p110γ-mediated negative regulation of IL-10 production was independent of kinase activity

Since a pan-PI3K inhibitor, wortmannin, did not mimic the effect of p110γ deficiency on CpG-induced IL-10 production, we next tested the effect of the p110γ-specific inhibitor, AS252424, on CpG-induced IL-10 production. C5a-induced Akt phosphorylation was completely abolished in p110γ$^{-/-}$ cells (Fig. 3A) [17]. The result confirmed that the C5a action is dependent on p110γ. AS252424 inhibited the C5a-induced Akt phosphorylation (Fig. 3A), indicating that the compound is a powerful tool for investigating the role of p110γ. Surprisingly, AS252424 did not cause an increase in CpG-induced IL-10 production in the wild type cells nor in p110γ$^{-/-}$ cells (Fig. 2B, C). These data suggest that the negative regulation of CpG-induced IL-10 production by p110γ was not dependent on its kinase activity.

CpG-induced IL-10 production was abolished in SCID mice

Recently, an indispensable role of DNA-PKcs in CpG-induced IL-10 production has been reported [7]. Since DNA-PKcs has a PI3K-like catalytic domain, the kinase activity is susceptible to wortmannin. As reported earlier [7], CpG-induced IL-10 production was defective in SCID mice (Fig. 4). Additionally, wortmannin inhibited significantly CpG-induced IL-10 production in wild type, whereas it did not affect this process in SCID mice (Fig. 4). This result suggests that wortmannin suppressed CpG-induced IL-10 production through inhibition of DNA-PKcs. By contrast, LPS-induced IL-10 production in SCID was identical to wild type with the same background mice (Fig. 4).

Co-localization of DNA-PKcs and CpG was increased in p110γ$^{-/-}$ cells

CpG is internalized via endocytosis and immediately moves into the lysosomal compartment [5,18,19]. A recent study reported that endosomal CpG preferentially induces IL-12 production, but,

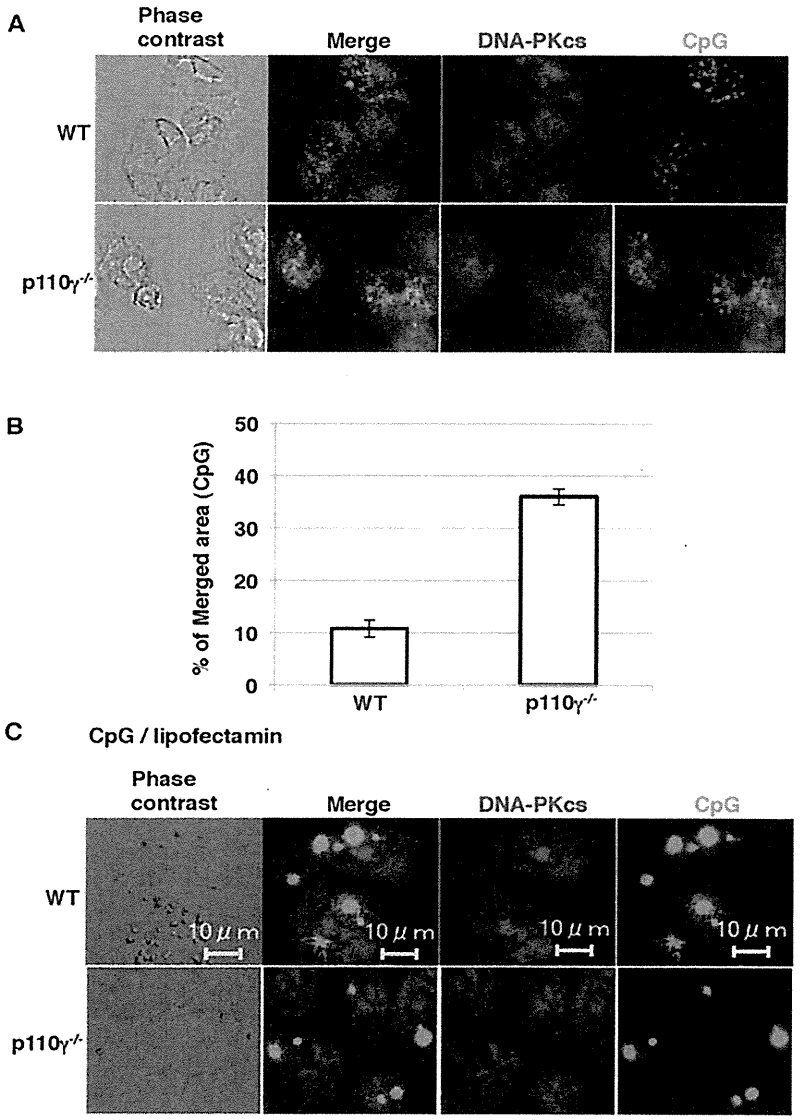

Figure 5. Increased co-localization of CpG and DNA-PKcs in p110γ$^{-/-}$ cells. Macrophages from wild type or p110γ$^{-/-}$ mice were incubated with 0.5 μM rhodamine-CpG (A) or rhodamine-CpG/lipofectamine LTX/Plus (C) for 60 min. The cells were washed, fixed, permeabilized, and stained with anti-DNA-PKcs antibody and Alexa 488-labeled secondary antibody. (B) The imaging data in (A) were quantified and shown as means ± SD.
doi:10.1371/journal.pone.0026836.g005

when released from the endosome, it associates with DNA-PKcs in cytoplasm and induces a greater amount of IL-10 [7]. Therefore, we hypothesized that CpG localized to the endosomal compartment in the wild type cells, and was more efficiently released into the cytosol in p110γ$^{-/-}$ cells. To quantify the co-localization of CpG and DNA-PKcs, macrophages were incubated with rhodamine-labeled CpG, fixed with formaldehyde, permeabilized, and incubated with anti-DNA-PKcs antibody. The merged area was calculated from the imaging data as described under materials and methods. The Co-localization area of CpG and DNA-PKcs was significantly increased in 110γ$^{-/-}$ cells (Fig. 5A, B). Interestingly, CpG complexed with cationic liposomes composed of Lipofectamine (LTX) and Plus reagent localized in large vesicles both in wild type and p110γ$^{-/-}$ cells, and scarcely co-localized with DNA-PKcs (Fig. 5C). Since wortmannin did not affect CpG uptake or localization of CpG or DNA-PKcs (data not shown), the PI3K inhibitor exclusively inhibits the kinase activity of DNA-PKcs.

Manipulation of CpG localization with cationic liposomes abolished the effect of p110γ deficiency on cytokine production

It seemed interesting to determine IL-10 production by CpG complexed with the lipofection reagent, which hardly co-localizes with DNA-PKcs. When cells were stimulated with this CpG/lipofection reagent, IL-10 production was decreased both in wild-type and p110γ$^{-/-}$ cells (Fig. 6). In addition, the augmentation of IL-10 production seen in p110γ$^{-/-}$ cells was completely abolished using this delivery system (Fig. 6).

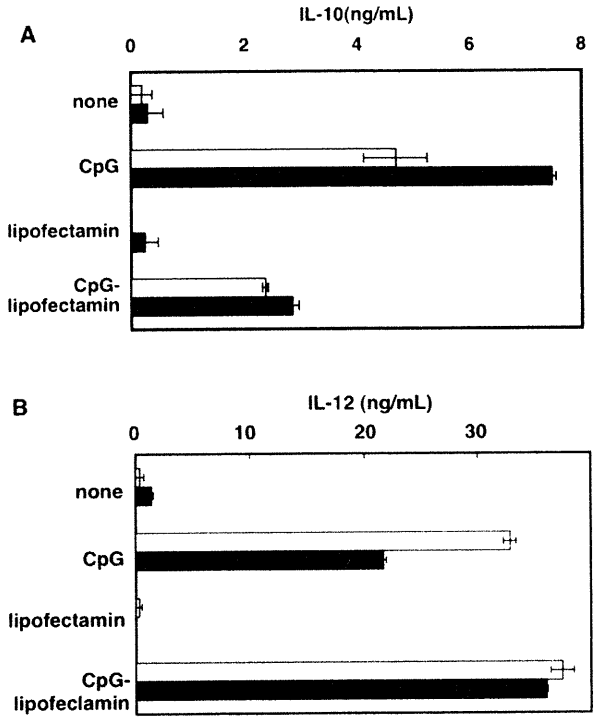

Figure 6. The effect of lipofection reagent on CpG-induced cytokine production. Macrophages from wild type (open bar) or p110γ$^{-/-}$ mice (solid bar) were incubated in 24-well plates with 200 ng/mL CpG or CpG/lipofectamine LTX/Plus reagent complex for 18 h. The amount of IL-10 (A) and IL-12 (B) in the medium was determined by ELISA. The values are the means ± SD of duplicate cultures from three independent experiments.
doi:10.1371/journal.pone.0026836.g006

CpG preferentially localized in the early endosome in wild type cells, and in lysosomes in p110γ$^{-/-}$ cells

We next tested the cellular delivery of CpG using an early endosome marker, EEA1, an endosome marker, dextran, and an acidic lysosome marker, LysoTracker. Quantitative analysis of microscopic images showed that more CpG merged with EEA1 and dextran in wild type cells than in p110γ$^{-/-}$ cells (Fig. 7A, B, D, E). By contrast, CpG preferentially merged with LysoTracker in p110γ$^{-/-}$ cells more than in wild-type cells (Fig. 7C, F). To further investigate the role of p110γ in CpG localization, Cos7 cells were transfected with p110γ and its mutant forms (unlike macrophages, Cos7 cells do not express p110γ). As shown in Fig. 8, most of the CpG was co-localized with LysoTracker in Cos7 cells transfected with vehicle alone, while scarcely co-localized with LysoTracker in the cells transfected with wild type p110γ. Interestingly, overexpression of a kinase-dead mutant of p110γ also inhibited the acidification of CpG-containing endosome. By contrast, the Ras-binding domain mutant form showed no effect on the CpG localization. These results suggest that PI3K p110γ play a role in endosomal acidification independent of its kinase activity. Since endosomal acidification is known to precede the endosomal leakage, acidification of CpG containing endosome may accelerate CpG translocation to the cytosol and the resultant association with DNA-PKcs to increase IL-10 production in macrophages.

CpG-induced but not LPS-induced IL-10 production was suppressed by inhibitors of endosomal acidification

Effect of chemical inhibitors of endosomal acidification [20] on CpG-induced IL-10 production was next examined. Both NH_4Cl and chloroquine strongly inhibited CpG-induced IL-10 production without affecting LPS-induced one (Fig. 9). The result supported our hypothesis that endosomal acidification is required for CpG-induced IL-10 production.

Discussion

In this study, we have identified a novel function of PI3K p110γ in the regulation of CpG localization. We have demonstrated this function using p110γ$^{-/-}$ macrophages and Cos7 cells transfected with p110γ. In macrophages, more CpG merged with the endosome markers, EEA1 and dextran, in wild type cells than in p110γ$^{-/-}$ cells, whereas preferentially merged with the acidic lysosome marker, LysoTracker, in p110γ$^{-/-}$ cells to a greater extent than in wild-type cells. In Cos7 cells, which do not express p110γ, most of the CpG was co-localized with LysoTracker, and scarcely co-localized with the dye in the cells transfected with p110γ. Another novel finding reported in this paper is that IL-10 production was increased specifically in p110γ$^{-/-}$ cells following CpG-stimulation. In p110γ$^{-/-}$ cells, the increased acidification of CpG containing endosomes and the resultant leakage of CpG to the cytosol, where DNA-PKcs resides, appears to be responsible for the modulation of cytokine production. For this reason, CpG-induced, but not LPS-induced, IL-10 production was almost completely abolished in SCID mice having mutations in DNA-PKcs. Furthermore, wortmannin, an inhibitor of DNA-PKcs, inhibited completely CpG-induced IL-10 production both in wild-type and in p110γ$^{-/-}$ cells. In addition to these, manipulation of the delivery system with cationic liposomes, which severely blocked the cytosolic delivery of CpG both in p110γ$^{-/-}$ and wild type cells, resulted in decreased IL-10 production. Finally, an intriguing point in this study is that the actions of p110γ on both the CpG delivery system and cytokine production were independent of its kinase activity.

Several kinase-independent functions of p110γ have been reported previously. Protein complexes containing p110γ are known to activate phosphodiesterase (PDE3B) in cardiomyocytes to degrade cAMP in a manner independent of its kinase activity [21,22]. Since increases in the cAMP level results in augmentation of TLR-mediated IL-12 production, with a decrease in IL-10 production [23], we had hypothesized that the increased IL-10 production in the absence of p110γ might be the result of elevated cAMP levels. To answer this question we tested some reagents known to increase cAMP, such as forskolin, prostaglandin E_2, 3-isobutyl-1-methylxanthin or dibutyryl cAMP in IL-10 production. Although these reagents more or less enhanced IL-10 production, the effect was not specific to CpG stimulation, but rather, was commonly observed in TLR-stimulation (data not shown). The other kinase-independent functions of p110γ are reported in vascular repair and platelet aggregation [22]. In addition, wild-type or the kinase-dead mutant of p110γ can block the growth of human colon cancer cells [24]. Although the mechanism of these kinase-independent actions of p110γ remains to be clarified, a scaffolding role for p110γ has been suggested [22].

p110γ$^{-/-}$ mice show severe defects in immune responses, and are protected completely against systemic anaphylaxis [25–28]. Additionally, in models of rheumatoid arthritis, systemic lupus erythematosus, and atherosclerosis, loss of p110γ activity results in protection against disease progression [29–31]. Since IL-10 is an anti-inflammatory cytokine, the increased IL-10 production in

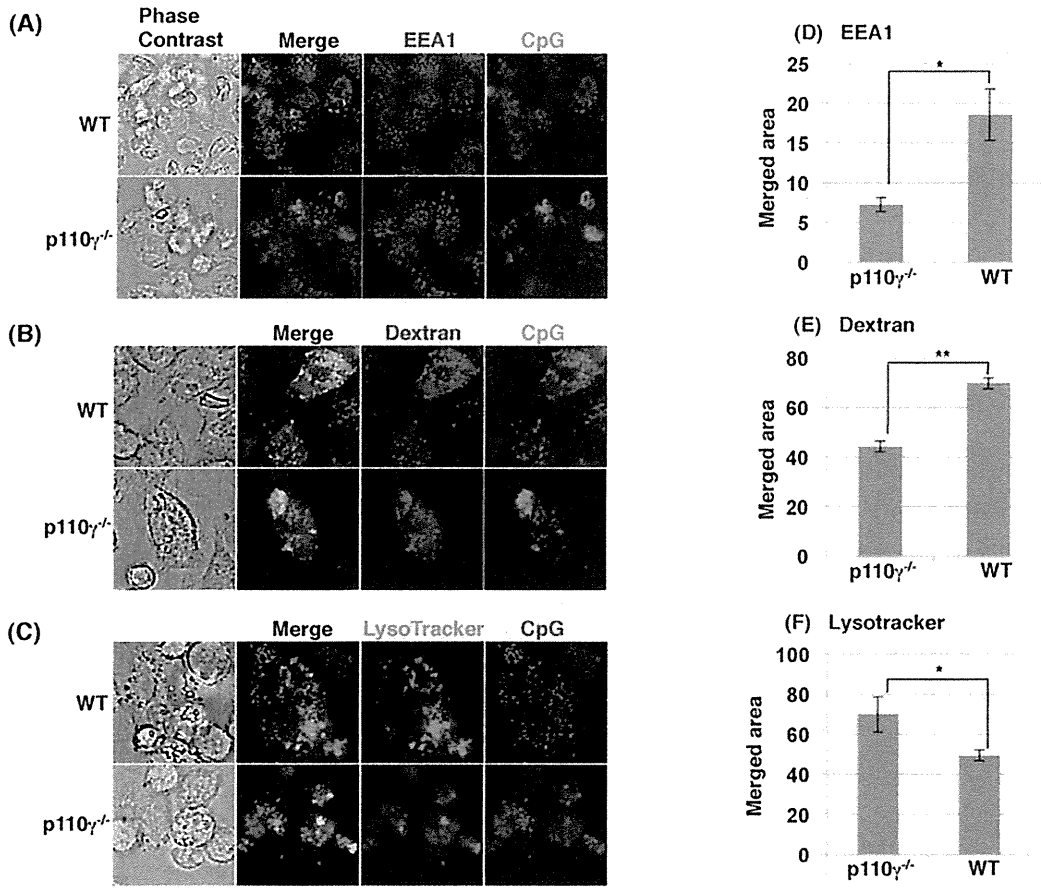

Figure 7. CpG localization in macrophages from wild type and p110γ$^{-/-}$ mice. Macrophages from wild type or p110γ$^{-/-}$ mice were incubated with 0.5 μM rhodamine-CpG (A, B) or FITC-CpG (C) for 30 min. FITC-dextran (1 mg/ml) (B) or LysoTracker red (50 nM) (C) was added simultaneously with CpG. The cells were washed and observed as live cells (B and C). In (A), the cells were fixed, permeabilized and stained with anti-EEA1 antibody and Alexa 488-labeled secondary antibody. The imaging data in (A, B, C) were quantified and shown as means ± SD in (D, E, F). *; $p<0.05$, **; $p<0.01$.
doi:10.1371/journal.pone.0026836.g007

p110γ-deficient cells may contribute, at least in a part, to protection against excessive inflammation. It is also likely that the increased IL-10 and decreased IL-12 production in p110γ$^{-/-}$ macrophage might explain partly the development of colorectal carcinomas in p110γ$^{-/-}$ mice [24], because the IL-12-mediated Th1 response favors effective anti-tumor immune responses [32]. Although further studies are needed to confirm the *in vivo* effect of p110γ on the translocation of CpG, our findings suggest that when p110γ is considered as a drug target for immune diseases [15,33,34], not only its lipid kinase function, but also its kinase-independent function should be considered.

Materials and Methods

Reagents

LPS (*E. coli* serotype 0111: B4), FITC-Dextran (average MW 40 kD) and C5a were from Sigma-Aldrich. Wortmannin was from Kyowa Medex (Tokyo, Japan). 5′-rhodamine-labeled, 5′-FITC-labeled and unlabeled CpG DNA (HPLC-purified phosphorothioate with the sequence of TCC ATG ACG TTC CTG ATG CT) were synthesized by Hokkaido System Science (Sapporo, Japan). LysoTracker Red was obtained from Lonza. Lipofectamine LTX Reagent, Plus Reagent and RPMI 1640 medium were from Invitrogen. The Protein Assay Kit was purchased from Bio-Rad. AS-252424 was from Cayman. Anti-pAkt (Ser473) antibody was from Cell Signalling, anti-Akt1/2 and anti-DNA-PKcs antibodies were from Santa Cruz, and anti-EEA1 was from GenScript. The IL-10 ELISA assay kit was from Biolegend.

Animals and cell isolation

All animal experiments were carried out in accordance with the NIH Guide for Care and Use of Laboratory Animals and approved by the animal care and use committee at Hiroshima University (Permit number: A08-23 and A08-46).

Female C57BL/6 mice, 8–12 weeks old, were purchased from Japan SLC, Inc. SCID, C.B-17/lcr$^{+/+}$, C.B-17/lcr-SCID/SCID mice were purchased from CLEA Japan. p110γ$^{-/-}$ mice on the C57BL/6 background were bred and maintained at Akita University (Akita, Japan). Thioglycollate-elicited macrophages were harvested from these mice. Briefly, mice were injected intra-peritoneally with 2 mL 3% thioglycollate broth. After 3 days, the peritoneal exudate cells were collected by washing the peritoneal cavity with ice-cold phosphate-buffered saline (PBS). The cells were seeded at about 5–10×10^5 cells/well in 24-well

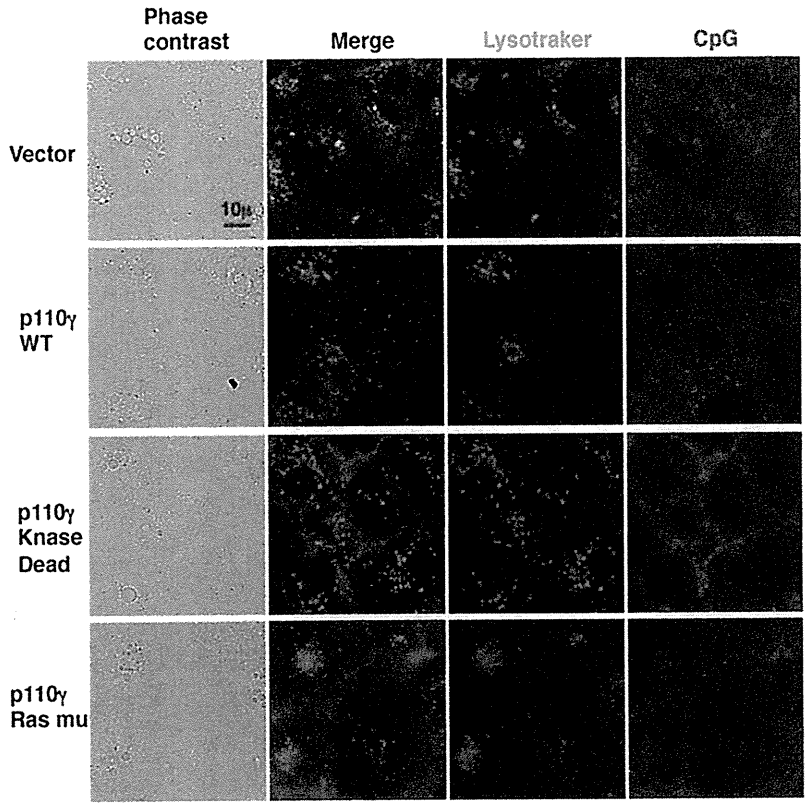

Figure 8. Effect of overexpression of p110γ on CpG localization in Cos7 cells. Cos7 cells were transfected with PI3K p110γor its mutant forms as described under materials and methods. Cells prepared in this manner were incubated with 50 nM LysoTracker red and 0.5 μM FITC-CpG for 30 min. The cells were washed and observed as live cells.
doi:10.1371/journal.pone.0026836.g008

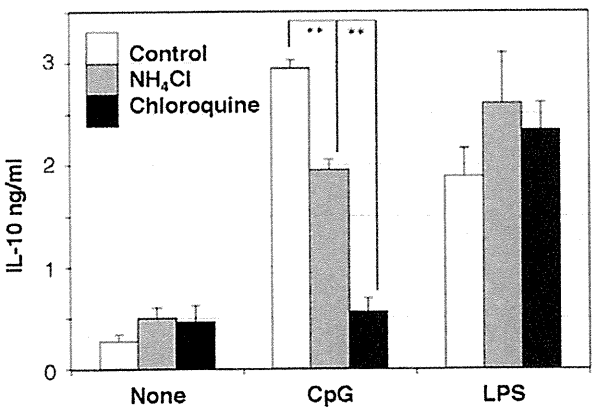

Figure 9. Effect of inhibitors of lysosomal acidification on IL-10 production. Macrophages from wild type mice were preincubated with 20 mM NH_4Cl, 50 μM Chloroquine or vehicle for 15 min, followed by the addition of 10 ng/mL LPS or 200 ng/mL CpG, for 18 h. The amount of IL-10 in the medium was determined by ELISA. The values are the means ± SD of duplicate cultures from three independent experiments. **; $p<0.01$.
doi:10.1371/journal.pone.0026836.g009

plates and incubated in humidified 5% CO_2 at 37°C for 1–2 h in RPMI 1640 medium supplemented with 10% fetal bovine serum (FBS) (MBL, Nagoya, Japan), to allow the cells to adhere to the wells. Non-adherent cells were removed by washing with PBS and the attached cells were used for experiments. Cos7 cells [35] were cultured in DMEM medium supplemented with 10% FBS.

Plasmids and transfection

Mammalian expression plasmids, pcDNA3 (Invitrogen), pcDNA3 containing wild-type p110γ, pcDNA3 containing a kinase-dead (R947P) mutant, or encoding a Ras binding site mutant (DASAA; T232D, K251A, K254S, K255A and K256A) [36] are transfected in to Cos7 cells using the Lipofectamine 2000 Reagent for 24 h.

Western blot

Cells were washed with PBS and lysed in 50 μL lysis buffer containing 25 mM Tris-HCl (pH 7.4), 0.5% Nonidet P-40, 150 mM NaCl, 1 mM sodium orthovanadate (Na_3VO_4), 1 mM EDTA, 0.1% BSA, 20 mM sodium fluoride, 1 mM phenylmethylsulfonyl fluoride, 2 μM leupeptin, 20 μM p-amidinophenylmethylsulfonyl fluoride, and 1 mM dithiothreitol. The cell lysates were centrifuged at 15,000 rpm for 10 min. Supernatants were collected and the protein concentration was determined using the Bio-Rad assay kit. Total cell lysates (100 μg protein) were mixed with 10 μL 5× sample buffer (62.5 mM Tris, pH 6.8, 1% SDS, 10% glycerol, 5% 2-mercaptoethanol, and 0.02% bromo-

phenol blue) and heated at 100°C for 5 min. The proteins were separated by SDS-PAGE and transferred electrophoretically onto a polyvinylidene difluoride (PVDF) membrane (Millipore). The membrane was blocked with 5% skim milk and incubated with the appropriate antibodies. Antibody binding was detected using a chemiluminescent substrate (Perkin-Elmer).

ELISA

Macrophage culture supernatants were used for the quantification of p40 and IL-10 using a commercially available ELISA kit.

Microscopy

Macrophages in multi-well, glass-bottom dishes (Greiner bio-one) were allowed to adhere for 60 min before the addition of rhodamine- or FITC-CpG. Where indicated, FITC-dextran or LysoTracker Red was added with CpG. The cells were washed four times to remove excess CpG before live cell imaging. Alternatively, the cells were fixed with 4% formaldehyde in PBS for 15 min, permeabilized with PBS containing 0.3% Triton X-100 and 0.5% BSA for 60 min, and incubated with anti-DNA-PKcs or anti-EEA1 at 4°C overnight. They were then incubated with Alexa 488-labeled goat anti-mouse IgG antibody $(Fab')_2$ for 2 h at room temperature. Cos7 cells were seeded into the culture wells a day before the transfection. The cells were incubated with LysoTracker red and FITC-CpG for 15 min as indicated. The cells were washed four times with PBS before imaging. Microscopic studies were performed using the Keyence BZ-9000 (Keyence, Osaka, Japan). The imaging data were analyzed by the BZ-H2A application. Values of (merged area)/(CpG area)×100 were determined from at least 5 imaging data, and the data are shown as the means ± SD. Statistical differences were determined at the level of $p<0.05$ or 0.01 with Student's t test.

Author Contributions

Conceived and designed the experiments: KH YK OH. Performed the experiments: KH YK HM MU YI. Analyzed the data: KH YK HM KN ST T. Seya MM OH. Contributed reagents/materials/analysis tools: KH ST T. Sasaki T. Seya. Wrote the paper: KH OH.

References

1. Krieg AM (2006) Therapeutic potential of Toll-like receptor 9 activation. Nat Rev Drug Discov 5: 471–484.
2. Wilson HL, Dar A, Napper SK, Marianela Lopez A, Babiuk LA, et al. (2006) Immune mechanisms and therapeutic potential of CpG oligodeoxynucleotides. Int Rev Immunol 25: 183–213.
3. Hemmi H, Takeuchi O, Kawai T, Kaisho T, Sato S, et al. (2000) A Toll-like receptor recognizes bacterial DNA. Nature 408: 740–745.
4. Bauer S, Kirschning CJ, Hacker H, Redecke V, Hausmann S, et al. (2001) Human TLR9 confers responsiveness to bacterial DNA via species-specific CpG motif recognition. Proc Natl Acad Sci U S A 98: 9237–9242.
5. Rutz M, Metzger J, Gellert T, Luppa P, Lipford GB, et al. (2004) Toll-like receptor 9 binds single-stranded CpG-DNA in a sequence- and pH-dependent manner. Eur J Immunol 34: 2541–2550.
6. Dragoi AM, Fu X, Ivanov S, Zhang P, Sheng L, et al. (2005) DNA-PKcs, but not TLR9, is required for activation of Akt by CpG-DNA. EMBO J 24: 779–789.
7. Yotsumoto S, Saegusa K, Aramaki Y (2008) Endosomal translocation of CpG-oligodeoxynucleotides inhibits DNA-PKcs-dependent IL-10 production in macrophages. J Immunol 180: 809–816.
8. Honda K, Ohba Y, Yanai H, Negishi H, Mizutani T, et al. (2005) Spatiotemporal regulation of MyD88-IRF-7 signalling for robust type-I interferon induction. Nature 434: 1035–1040.
9. Fukao T, Tanabe M, Terauchi Y, Ota T, Matsuda S, et al. (2002) PI3K-mediated negative feedback regulation of IL-12 production in DCs. Nat Immunol 3: 875–881.
10. Hazeki K, Kinoshita S, Matsumura T, Nigorikawa K, Kubo H, et al. (2006) Opposite effects of wortmannin and 2-(4-morpholinyl)-8-phenyl-1(4H)-benzopyran-4-one hydrochloride on toll-like receptor-mediated nitric oxide production: negative regulation of nuclear factor-{kappa}B by phosphoinositide 3-kinase. Mol Pharmacol 69: 1717–1724.
11. Kuo CC, Lin WT, Liang CM, Liang SM (2006) Class I and III phosphatidylinositol 3'-kinase play distinct roles in TLR signaling pathway. J Immunol 176: 5943–5949.
12. Ishii KJ, Takeshita F, Gursel I, Gursel M, Conover J, et al. (2002) Potential role of phosphatidylinositol 3 kinase, rather than DNA-dependent protein kinase, in CpG DNA-induced immune activation. J Exp Med 196: 269–274.
13. Guiducci C, Ghirelli C, Marloie-Provost MA, Matray T, Coffman RL, et al. (2008) PI3K is critical for the nuclear translocation of IRF-7 and type I IFN production by human plasmacytoid predendritic cells in response to TLR activation. J Exp Med 205: 315–322.
14. Cao W, Manicassamy S, Tang H, Kasturi SP, Pirani A, et al. (2008) Toll-like receptor-mediated induction of type I interferon in plasmacytoid dendritic cells requires the rapamycin-sensitive PI(3)K-mTOR-p70S6K pathway. Nat Immunol 9: 1157–1164.
15. Marone R, Cmiljanovic V, Giese B, Wymann MP (2008) Targeting phosphoinositide 3-kinase: moving towards therapy. Biochim Biophys Acta 1784: 159–185.
16. Saegusa K, Yotsumoto S, Kato S, Aramaki Y (2007) Phosphatidylinositol 3-kinase-mediated regulation of IL-10 and IL-12 production in macrophages stimulated with CpG oligodeoxynucleotide. Mol Immunol 44: 1323–1330.
17. Sasaki T, Irie-Sasaki J, Jones RG, Oliveira-dos-Santos AJ, Stanford WL, et al. (2000) Function of PI3Kgamma in thymocyte development, T cell activation, and neutrophil migration. Science 287: 1040–1046.
18. Hacker H, Mischak H, Miethke T, Liptay S, Schmid R, et al. (1998) CpG-DNA-specific activation of antigen-presenting cells requires stress kinase activity and is preceded by non-specific endocytosis and endosomal maturation. EMBO J 17: 6230–6240.
19. Latz E, Schoenemeyer A, Visintin A, Fitzgerald KA, Monks BG, et al. (2004) TLR9 signals after translocating from the ER to CpG DNA in the lysosome. Nat Immunol 5: 190–198.
20. Misinzo G, Delputte PL, Nauwynck HJ (2007) Inhibition of endosome-lysosome system acidication enhances porcine circovirus 2 infection of porcine epithelial cells. J Virol 82: 1128–1135.
21. Patrucco E, Notte A, Barberis L, Selvetella G, Maffei A, et al. (2004) PI3Kgamma modulates the cardiac response to chronic pressure overload by distinct kinase-dependent and -independent effects. Cell 118: 375–387.
22. Hirsch E, Braccini L, Ciraolo E, Morello F, Perino A (2009) Twice upon a time: PI3K's secret double life exposed. Trends Biochem Sci 34: 244–248.
23. Koga K, Takaesu G, Yoshida R, Nakaya M, Kobayashi T, et al. (2009) Cyclic adenosine monophosphate suppresses the transcription of proinflammatory cytokines via the phosphorylated c-Fos protein. Immunity 30: 372–383.
24. Sasaki T, Irie-Sasaki J, Horie Y, Bachmaier K, Fata JE, et al. (2000) Colorectal carcinomas in mice lacking the catalytic subunit of PI(3)Kgamma. Nature 406: 897–902.
25. Suire S, Coadwell J, Ferguson GJ, Davidson K, Hawkins P, et al. (2005) p84, a new Gbetagamma-activated regulatory subunit of the type IB phosphoinositide 3-kinase p110gamma. Curr Biol 15: 566–570.
26. Voigt P, Dorner MB, Schaefer M (2006) Characterization of p87PIKAP, a novel regulatory subunit of phosphoinositide 3-kinase gamma that is highly expressed in heart and interacts with PDE3B. J Biol Chem 281: 9977–9986.
27. Stephens LR, Eguinoa A, Erdjument-Bromage H, Lui M, Cooke F, et al. (1997) The G beta gamma sensitivity of a PI3K is dependent upon a tightly associated adaptor, p101. Cell 89: 105–114.
28. Rommel C, Camps M, Ji H (2007) PI3K delta and PI3K gamma: partners in crime in inflammation in rheumatoid arthritis and beyond? Nat Rev Immunol 7: 191–201.
29. Barber DF, Bartolome A, Hernandez C, Flores JM, Redondo C, et al. (2005) PI3Kgamma inhibition blocks glomerulonephritis and extends lifespan in a mouse model of systemic lupus. Nat Med 11: 933–935.
30. Chang JD, Sukhova GK, Libby P, Schvartz E, Lichtenstein AH, et al. (2007) Deletion of the phosphoinositide 3-kinase p110gamma gene attenuates murine atherosclerosis. Proc Natl Acad Sci U S A 104: 8077–8082.
31. Camps M, Ruckle T, Ji H, Ardissone V, Rintelen F, et al. (2005) Blockade of PI3Kgamma suppresses joint inflammation and damage in mouse models of rheumatoid arthritis. Nat Med 11: 936–943.
32. Fukao T, Koyasu S (2003) PI3K and negative regulation of TLR signaling. Trends Immunol 24: 358–363.
33. Ohashi PS, Woodgett JR (2005) Modulating autoimmunity: pick your PI3 kinase. Nat Med 11: 924–925.
34. Ruckle T, Schwarz MK, Rommel C (2006) PI3Kgamma inhibition: towards an 'aspirin of the 21st century'? Nat Rev Drug Discov 5: 903–918.
35. Gluzman Y (1981) SV40-transformed simian cells support the replication of early SV40 mutants. Cell 23: 175–182.
36. Suire S, Condliffe AM, Ferguson GJ, Ellson CD, Guillou H, et al. (2006) Gbetagammas and the Ras binding domain of p110gamma are both important regulators of PI(3)Kgamma signalling in neutrophils. Nat Cell Biol 8: 1303–1309.

JVI
Journals.ASM.org

The Toll-Like Receptor 3-Mediated Antiviral Response Is Important for Protection against Poliovirus Infection in Poliovirus Receptor Transgenic Mice

Yuko Abe,[a] Ken Fujii,[a] Noriyo Nagata,[b] Osamu Takeuchi,[c] Shizuo Akira,[c] Hiroyuki Oshiumi,[d] Misako Matsumoto,[d] Tsukasa Seya,[d] and Satoshi Koike[a]

Neurovirology Project, Tokyo Metropolitan Institute of Medical Science, 2-1-6 Kamikitazawa, Setagaya-ku, Tokyo 156-8506, Japan[a]; Department of Pathology, National Institute of Infectious Diseases, 4-7-1 Gakuen, Musashimurayama, Tokyo 208-0011, Japan[b]; Laboratory of Host Defense, WPI Immunology Frontier Research Center (IFReC), Osaka University, 3-1 Yamada-oka, Suita, Osaka 565-0871, Japan[c]; and Department of Microbiology and Immunology, Hokkaido University Graduate School of Medicine, Kita 15, Nishi 7, Kita-ku, Sapporo 060-8638, Japan[d]

RIG-I-like receptors and Toll-like receptors (TLRs) play important roles in the recognition of viral infections. However, how these molecules contribute to the defense against poliovirus (PV) infection remains unclear. We characterized the roles of these sensors in PV infection in transgenic mice expressing the PV receptor. We observed that alpha/beta interferon (IFN-α/β) production in response to PV infection occurred in an MDA5-dependent but RIG-I-independent manner in primary cultured kidney cells *in vitro*. These results suggest that, similar to the RNA of other picornaviruses, PV RNA is recognized by MDA5. However, serum IFN-α levels, the viral load in nonneural tissues, and mortality rates did not differ significantly between MDA5-deficient mice and wild-type mice. In contrast, we observed that serum IFN production was abrogated and that the viral load in nonneural tissues and mortality rates were both markedly higher in TIR domain-containing adaptor-inducing IFN-β (TRIF)-deficient and TLR3-deficient mice than in wild-type mice. The mortality rate of MyD88-deficient mice was slightly higher than that of wild-type mice. These results suggest that multiple pathways are involved in the antiviral response in mice and that the TLR3-TRIF-mediated signaling pathway plays an essential role in the antiviral response against PV infection.

Poliovirus (PV), which belongs to the genus *Enterovirus* in the family *Picornaviridae*, is the causative agent of poliomyelitis (38). The host range of PV is restricted to primates (18). This species' tropism is determined primarily by the cellular PV receptor (PVR; CD155), which gives the virus access to susceptible cells (14–16, 20). Mice are generally not susceptible to PV. However, transgenic mice expressing human PVR (PVR-tg mice) become susceptible to PV and develop a paralytic disease similar to human poliomyelitis after the administration of PV intravenously, intraperitoneally, intracerebrally, or intramuscularly but not orally (26, 40). PV shows a neurotropic phenotype in both humans and PVR-tg mice. PV preferentially replicates in neurons, especially in motor neurons in the anterior or ventral horn of the spinal cord and in the brainstem. However, the efficiency of PV replication is low in nonneural tissues (4, 25). We previously found that innate immune responses that are mediated by type I interferons (IFNs) play important roles in controlling viral replication in nonneural tissues and in the mortality rates of PVR-tg mice (19). In PVR-tg mice deficient in IFNAR1, PV efficiently replicates in nonneural tissues such as the liver, pancreas, and spleen, which are not normal targets of PV. IFNAR1-deficient mice die after the inoculation of a small amount of PV by peripheral routes. The results suggest that the type I IFN response forms an innate immune barrier that prevents PV replication in nonneural tissues and subsequent PV invasion of the central nervous system (CNS). This response therefore plays important roles in the tissue tropism and pathogenicity of PV (25).

The sensors that are involved in the production of type I IFNs in response to RNA viral infections have been recently identified and characterized (1, 46–48). The RIG-I-like receptors (RLRs) retinoic-acid-inducible gene 1 (RIG-I) and melanoma differentiation-associated gene 5 (MDA5) are expressed in the cytoplasm of all cell types, with the exception of plasmacytoid dendritic cells (pDCs). RIG-I and MDA5 have RNA binding domains and differentially recognize specific characteristics of nonself viral RNAs (17, 22, 36, 37). In addition, RLRs have DExD/H box RNA helicase domains (51) that activate downstream signaling pathways resulting in the activation of IFN regulatory factor 3 (IRF-3) and IRF-7 (53). TLR3 and TLR7 are the sensors for viral double-stranded RNA (dsRNA) and single-stranded RNA, respectively (2, 8, 12). TLR3 is expressed in the endosome of macrophages and conventional dendritic cells (DCs) (28) but not in pDCs. TLR3 is also expressed in a variety of epithelial cells, including airway, uterine, corneal, vaginal, cervical, biliary, and intestinal epithelial cells, which may function as efficient barriers to infection. The TLR3-mediated signaling pathway is transmitted through Toll–interleukin-1 (IL-1) receptor (TIR)-containing adaptor molecule 1, which is also known as TIR domain-containing adaptor inducing IFN-β (TRIF), and finally results in the activation of IRF3 and IRF7 (13, 34, 51). TLR7 is specifically expressed in the endosome of pDCs and contributes to the production of a large amount of IFNs in response to many RNA virus infections (5, 7). TLR7 signaling is mediated by the adaptor molecule myeloid differentiation factor 88 (MyD88). These sensors do not contribute equally

Received 29 May 2011 Accepted 20 October 2011
Published ahead of print 9 November 2011
Address correspondence to Satoshi Koike, koike-st@igakuken.or.jp.

doi:10.1128/JVI.05245-11

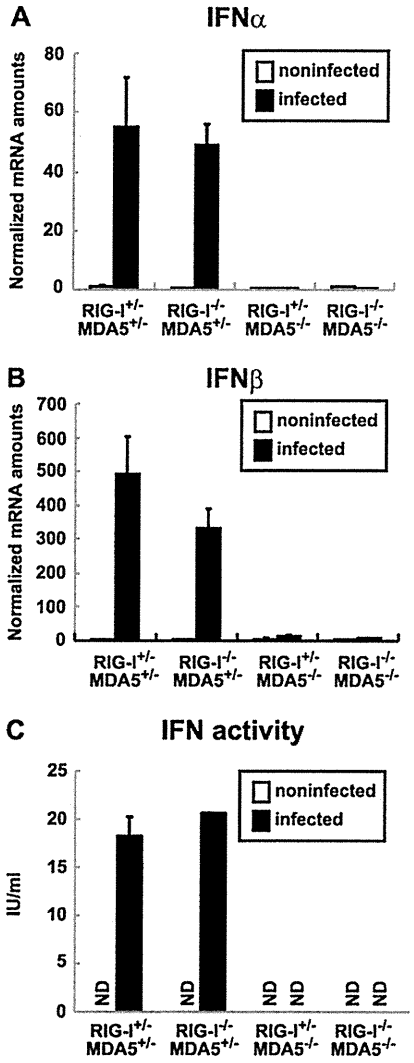

FIG 1 Production of IFNs in primary cultured kidney cells prepared from RIG-I- and MDA5-deficient mice. Kidney cells were pretreated with 100 U of IFN-β for 2 h and infected with PV at an MOI of 10. RNA was prepared from the infected cells at 6 hpi. The amounts of IFN-α mRNA (A) and IFN-β mRNA (B) were determined using quantitative real-time PCR. Cells were prepared in duplicate, and the experiments were repeated three times. Representative data are shown. The amount of IFN activity in the supernatant of infected kidney cells at 8 hpi was determined by the cytopathic effect dye uptake method using L929 cells (C). ND, not detected.

to the antiviral response to each viral infection. The type I IFN production that is induced by these sensors occurs in a virus-specific and cell-specific manner (21, 23). For example, RIG-I plays an important role in the antiviral response to Newcastle disease virus, influenza A virus, Sendai virus, vesicular stomatitis virus, Japanese encephalitis virus, and hepatitis C virus. However, MDA5 is important in the response to infection with picornaviruses, such as encephalomyocarditis virus (EMCV) (10, 23). Although RNA viruses produce dsRNA during the replication step, the protective effect of the TLR3-mediated pathway is not clear (9). In a previous study, TLR3 expression was found to cause severe encephalitis in West Nile virus (WNV) infection (50). How these sensor molecules contribute to the recognition of PV infection is not understood. The aim of the present study was to determine the role of these sensors in the response to PV infection in transgenic mice expressing human PVR. We generated PVR-tg mice deficient in these sensor and adaptor molecules. Our results demonstrate that the MDA5-, TRIF- and MyD88-mediated pathways contribute to the antiviral response against PV infection and that the TLR3-TRIF-mediated pathway plays a pivotal role in this response.

MATERIALS AND METHODS

Cells and viruses. An AGMK cell line, JVK-03 (24), was maintained in Eagle's minimum essential medium containing 5% fetal bovine serum. PV type I Mahoney, a strain derived from the infectious cDNA clone pOM, was used in this study (45). The virus was propagated in JVK-03, and the viral titer was determined using the plaque assay. Primary cultured kidney cells were prepared from transgenic and knockout mice as previously described (54).

Transgenic and knockout mice and infection experiments. All experiments using mice were performed in accordance with the Guidelines for the Care and Use of Laboratory Animals of the Tokyo Metropolitan Institute of Medical Science. ICR-PVRTg21 mice (26) were mated with RIG-I$^{-/-}$ and/or MDA5$^{-/-}$ mice (21) in the ICR background because it is difficult to maintain RIG-I$^{-/-}$ mice in other genetic backgrounds. We mated mice and obtained littermates with the genotypes RIG-I$^{+/-}$ MDA5$^{+/-}$, RIG-I$^{-/-}$ MDA5$^{+/-}$, RIG-I$^{+/-}$ MDA5$^{-/-}$, and RIG-I$^{-/-}$ MDA5$^{-/-}$ to use in experiments. C57BL/6 (B6)-PVRTg21 mice were mated with MDA5$^{-/-}$ mice, TRIF$^{-/-}$ mice, MyD88$^{-/-}$ mice, and TLR3$^{-/-}$ mice (51) in the B6 background (backcrossed 7 to 10 times). IFNAR1$^{-/-}$ PVR-tg mice were previously described (19). Because all of the mice that were used in the present study were in the PVR-tg background, we omitted the notation "PVR-tg" for simplicity in this report. Six- to 7-week-old mice were used for infection experiments. The survival and clinical symptoms of the mice were observed daily for 3 weeks. At the first sign of severe neurological symptoms, the mice were sacrificed as a humane endpoint.

Measurement of IFN levels. IFN-α levels in the sera were determined using an enzyme-linked immunosorbent assay (ELISA). The ELISA kit for IFN-α was purchased from PBL Biochemical Laboratories. Mouse IFN activity in the supernatants of PV-infected kidney cells was measured by the cytopathic effect dye uptake method using L929 cells (54, 55). Recombinant mouse IFN-β (Toray) was used as the standard for unit definition.

Quantitative real-time reverse transcription (RT)-PCR. RNA was isolated from the tissues of infected mice or infected cells using the Isogen RNA extraction kit (Nippon Gene). DNase I treatment and cDNA synthesis were performed as previously described (54). The amounts of the mRNAs for IFN-α, IFN-β, OAS1a, and IRF-7 were determined using real-time RT-PCR with an ABI Prism 7500 (Applied Biosystems) as previously described (54).

RESULTS

IFN production in primary cultured kidney cells is dependent on MDA5. We examined whether, similar to EMCV infection, PV infection is recognized by MDA5 *in vitro*. We mated PVR-tg mice with MDA5-deficient and RIG-I-deficient mice to generate RIG-I$^{+/-}$ MDA5$^{+/-}$, RIG-I$^{-/-}$ MDA5$^{+/-}$, RIG-I$^{+/-}$ MDA5$^{-/-}$, and RIG-I$^{-/-}$ MDA5$^{-/-}$ mice in the ICR background. We prepared primary cultured kidney cells from mice with these genotypes to determine the role of RLRs. After cultivation for approximately 1 week, the cells that became confluent were infected with PV at a multiplicity of infection (MOI) of 10. RNA was recovered from the infected cells at 6 hpi, and the amounts of the mRNAs for IFN-α and IFN-β were determined using real-time RT-PCR. Kid-

ney cells that were not pretreated with IFN-β before PV infection showed rapid cytopathic effect progression and did not produce IFN mRNA (data not shown). This result is consistent with our previous observations (54). We therefore pretreated cells with 100 U of IFN-β for 2 h and infected them with PV. As we reported previously, the IFN-treated kidney cells became resistant to PV infection, PV replication was severely inhibited, and IFN production was observed (54). Under this condition, we determined the sensor responsible for IFN production. We observed the induction of both IFN-α (Fig. 1A) and IFN-β mRNAs (Fig. 1B) in cells that were isolated from RIGI-I$^{+/-}$ MDA5$^{+/-}$ mice and RIGI-I$^{-/-}$ MDA5$^{+/-}$ mice but not from RIGI-I$^{+/-}$ MDA5$^{-/-}$ mice or RIGI-I$^{-/-}$ MDA5$^{-/-}$ mice. The induced IFN proteins were not detected by ELISA due to a very small amount of IFNs produced in the supernatants. However, IFN activity was detected in the supernatants of PV-infected kidney cells prepared from RIGI-I$^{+/-}$ MDA5$^{+/-}$ mice and RIGI-I$^{-/-}$ MDA5$^{+/-}$ mice but not from RIGI-I$^{+/-}$ MDA5$^{-/-}$ mice or RIGI-I$^{-/-}$ MDA5$^{-/-}$ mice using the cytopathic effect dye uptake method (Fig. 1C). These results suggest that PV infection is recognized by MDA5 but not RIG-I in primary murine kidney cells, which is consistent with previous reports demonstrating that MDA5 is essential for the detection of picornaviruses (10, 23). However, MDA5-mediated IFN production was observed only when cells had been primed with a low dose of IFNs.

IFN responses of MDA5-deficient mice are not significantly different from those of wild-type mice. We hypothesized that MDA5 plays an important role in the type I IFN response upon PV infection *in vivo*. We examined the serum IFN-α levels in PVR-tg mice intravenously infected with 2×10^7 PFU of PV using ELISA. Their serum IFN-α level was initially observed at 9 hpi, peaked at 12 hpi, and began to decline at 24 hpi (Fig. 2A). We then determined the serum IFN-α levels of the knockout mice at 12 hpi. Unexpectedly, similar serum IFN-α levels were detected in RIG-I$^{+/-}$ MDA5$^{+/-}$, RIG-I$^{+/-}$ MDA5$^{-/-}$, RIG-I$^{-/-}$ MDA5$^{+/-}$, and RIG$^{-/-}$ MDA5$^{-/-}$ mice infected with PV (Fig. 2B).

We monitored the induction of mRNAs for the IFN-stimulated genes (ISGs), OAS1a (Fig. 3A) and IRF-7 (Fig. 3B), in the brain, spinal cord, liver, spleen, and kidney using real-time RT-PCR. Among the organs tested, the expression levels of these ISGs were the highest in the spleen. However, the expression profiles of these genes were essentially the same in all organs. In accordance with the elevated serum IFN levels, the induction of ISGs in various organs was observed in all mice (Fig. 3A and B). The results suggest that MDA5 does not play a critical role in IFN production and subsequent ISG induction in response to PV infection *in vivo*.

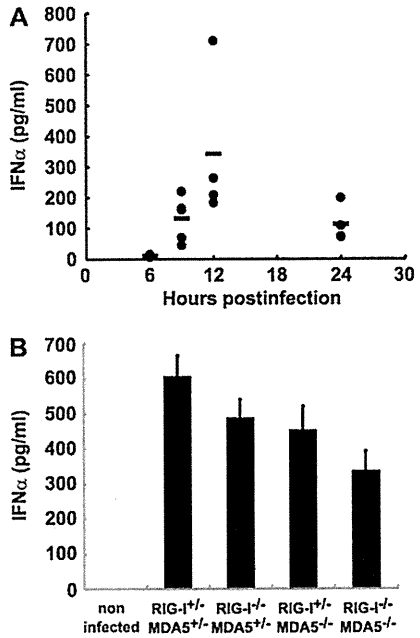

FIG 2 Production of serum IFN-α in RIG-I- and MDA5-deficient mice. (A) Time course of IFN-α levels in serum. PVR-tg mice in the B6 background (n = 4 or n = 5) were intravenously infected with 2×10^7 PFU of PV. Serum samples were collected at the indicated time points, and the concentration of IFN-α was determined using ELISA. (B) IFN-α levels of RIG-I- and MDA5-deficient mice in the ICR background (n = 8) at 12 hpi were compared. The experiments were repeated twice, and representative data are shown.

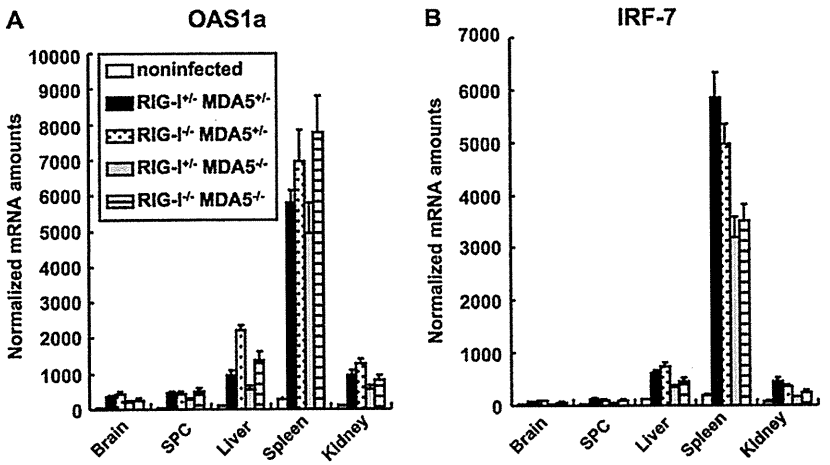

FIG 3 ISG induction in RIG-I- and MDA5-deficient mice. Mice (n = 4) were intravenously infected with 2×10^7 PFU of PV. At 12 hpi, RNA was isolated from the indicated tissues of the infected mice and OAS1a (A) and IRF-7 (B) mRNA levels were determined using quantitative real-time PCR. The experiments were repeated twice, and representative data are shown. SPC, spinal cord.

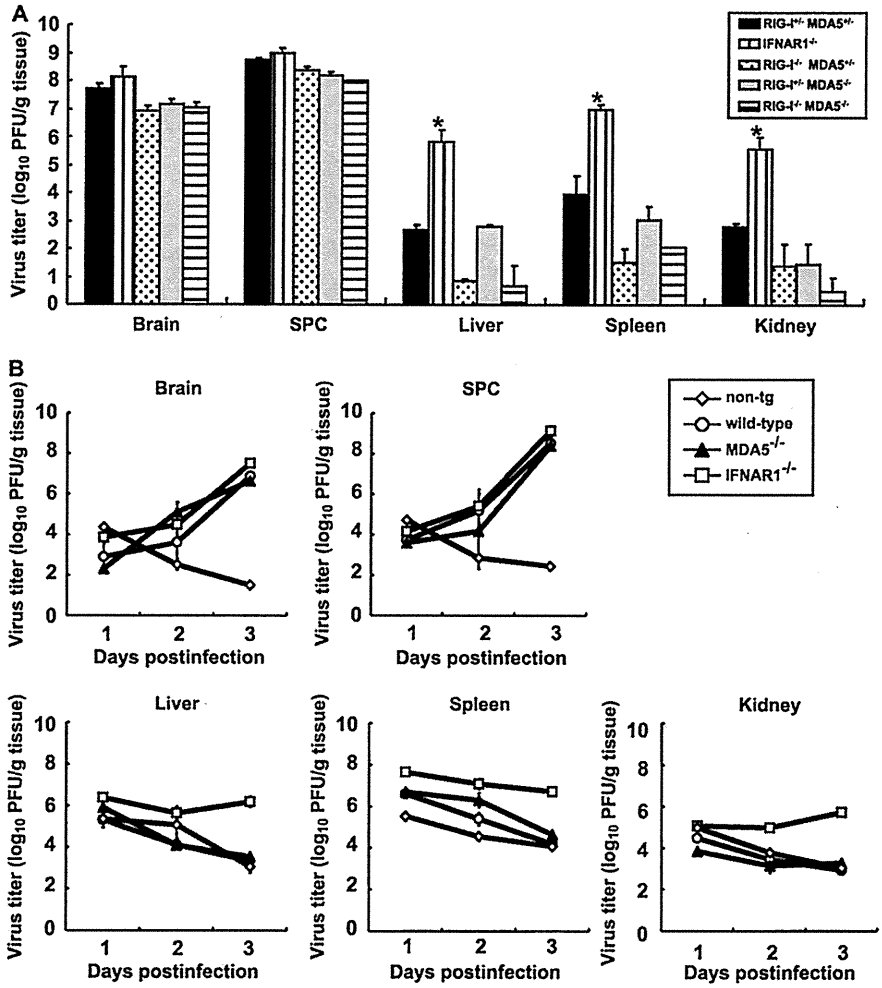

FIG 4 (A) PV replication in RIG-I- and MDA5-deficient mice. RIGI-$I^{+/-}$ $MDA5^{+/-}$, RIGI-$I^{-/-}$ $MDA5^{+/-}$, RIGI-$I^{-/-}$ $MDA5^{+/-}$, and RIGI-$I^{-/-}$ $MDA5^{-/-}$ mice in the ICR background and $IFNAR1^{-/-}$ mice in the B6 background ($n = 3$) were intravenously infected with 2×10^7 PFU of PV. Infected mice were paralyzed or dead at 3 to 5 days postinfection. The tissues of the paralyzed mice were collected, and the viral titers were determined using a plaque assay (*, $P < 0.01$ by t test compared to RIGI-$I^{+/-}$ $MDA5^{+/-}$ mice). (B) PV replication kinetics in MDA5-deficient mice. Nontransgenic (non-tg) mice, wild-type mice, $MDA5^{-/-}$ mice, and $IFNAR1^{-/-}$ mice in the B6 background ($n = 3$) were infected as described above. Tissues were collected daily, and viral titers were determined. SPC, spinal cord.

PV replication in nonneural tissues and mortality rates of mice deficient in RIG-I-like receptors. We have previously shown that the IFN-α/β response forms an innate immune barrier to prevent PV replication in nonneural tissues and PV invasion of the CNS (19, 25). Therefore, we evaluated PV replication in neural and nonneural tissues in RLR-deficient mice. The mice were infected with 2×10^7 PFU of PV, which is approximately 100 times higher than the 50% lethal doses for all mouse strains. The infected mice showed paralysis by 3 to 5 days postinfection. The brain, spinal cord, liver, spleen, and kidney of the paralyzed mice were recovered, and their viral titers were determined (Fig. 4A). PV was recovered from the CNS of the paralyzed mice almost equally among the genotypes. The viral titers recovered from the liver, spleen, and kidney of $IFNAR1^{-/-}$ mice were significantly higher than those of wild-type mice, as previously described (19). However, PV titers that were recovered from these organs of RIG-$I^{-/-}$ $MDA5^{+/-}$, RIG-$I^{+/-}$ $MDA5^{-/-}$, and RIG-$I^{-/-}$ $MDA5^{-/-}$ mice were as low as or lower than those in the organs of RIG-$I^{+/-}$ $MDA5^{+/-}$ mice. We then examined virus replication kinetics using nontransgenic mice, wild-type mice, $IFNAR^{-/-}$ mice, and $MDA5^{-/-}$ mice in the B6 background (Fig. 4B). The viral load in the CNS increased in a similar fashion among the transgenic mouse strains. However, the viral load kinetics in the liver, spleen, and kidney of wild-type and $MDA5^{-/-}$ mice were similar to those of nontransgenic mice. The values for nontransgenic mice indicate the kinetics of clearance of inoculated virus. The results indicated that PV replication was severely inhibited in the liver, spleen, and kidney of wild-type and $MDA5^{-/-}$ mice. This inhibition correlated well with the induction of serum IFNs in $MDA5^{-/-}$ mice (Fig. 2). The PV antigen was detected in neurons in the CNS but not in other tissues in all knockout mice (Table 1). This result indicates that the lack of RLRs did not alter the tissue tropism of PV. These data suggest that inhibition of PV replication in nonneural tissues is not dependent on RLRs and that MDA5-independent mechanisms are the major contributors in controlling PV replication.

We examined the mortality rates of RIG-$I^{+/-}$ $MDA5^{+/-}$, RIG-$I^{-/-}$ $MDA5^{+/-}$, RIG-$I^{+/-}$ $MDA5^{-/-}$, and RIG-$I^{-/-}$ $MDA5^{-/-}$

TABLE 1 PV antigens in RIG-I- and MDA5-deficient mice

Organ or tissue	No. of PV antigen-positive mice/no. of mice tested			
	RIG-I$^{+/-}$ MDA5$^{+/-}$	RIG-I$^{-/-}$ MDA5$^{+/-}$	RIG-I$^{+/-}$ MDA5$^{-/-}$	RIG-I$^{-/-}$ MDA5$^{-/-}$
Brain	4/4	3/3	4/4	4/4
Spinal cord	4/4	3/3	4/4	4/4
Heart	0/4	0/3	0/4	0/4
Lung	0/4	0/3	0/4	0/4
Liver	0/4	0/3	0/4	0/4
Kidney	0/4	0/3	0/4	0/4
Spleen	0/4	0/3	0/4	0/4
Pancreas	0/4	0/3	0/4	0/4
Intestine	0/4	0/3	0/4	0/4
Adipose tissue	0/4	0/3	0/4	0/4

mice in the ICR background after intravenous infection with PV at 10^3, 10^4, and 10^5 PFU (Fig. 5A, B, and C). The mortality rates of these mice did not differ significantly from each other. We observed that the mortality rates of RIG-I$^{+/-}$ MDA5$^{-/-}$ mice that were inoculated with 10^4 PFU of PV was slightly higher than the mice of other genotypes. However, significant differences were not observed in mice that were inoculated with the other doses. Similar experiments were performed using MDA5$^{-/-}$ and MDA5$^{+/-}$ mice in the B6 background (Fig. 5D, E, and F). We did not observe significant differences between the MDA5$^{-/-}$ and MDA5$^{+/-}$ mice. The mortality rate of MDA5$^{-/-}$ mice was slightly higher than that of MDA5$^{+/-}$ mice that were inoculated with 10^5 PFU of PV. However, the opposite trend was observed when mice

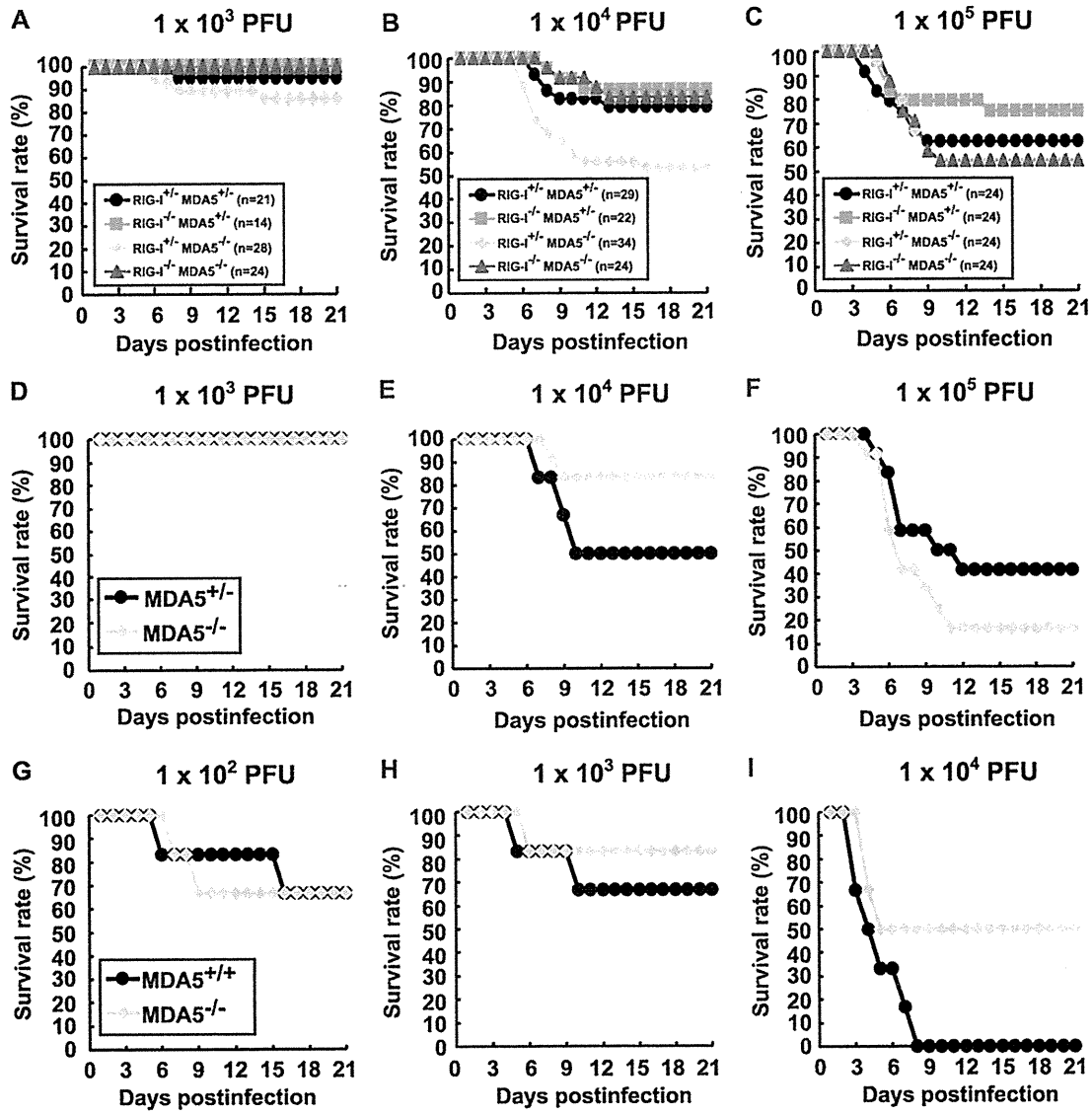

FIG 5 Mortality rates of RIG-I- and MDA5-deficient mice. Littermates of the genotypes indicated were obtained by mating RIGI-I$^{+/-}$ MDA5$^{+/-}$ and RIGI-I$^{-/-}$ MDA5$^{-/-}$ mice in the ICR background. The mice were infected intravenously with 10^3 (A), 10^4 (B), or 10^5 (C) PFU of PV. The results shown are the sums of several independent experiments. The total numbers of mice of the different genotypes that were used are boxed, and the doses used are shown at the top. Littermates of MDA5$^{+/-}$ and MDA5$^{-/-}$ mice were obtained in the B6 background. The mice (n = 12) were intravenously infected with 10^3 (D), 10^4 (E), or 10^5 (F) of PV. MDA5$^{+/+}$ and MDA5$^{-/-}$ mice (n = 6) were intracerebrally infected with 10^2 (G), 10^3 (H), or 10^4 (I) PFU of PV, respectively. We monitored the survival rates of the mice for 3 weeks after infection.

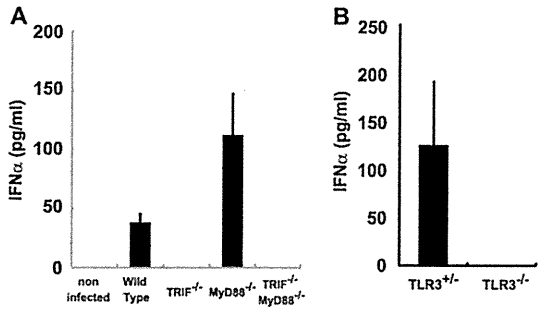

FIG 6 Production of serum IFN-α in TRIF-, MyD88-, and TLR3-deficient mice. Mice (n = 3 or 8) were intravenously infected with 10^7 PFU of PV. IFN-α levels of TRIF- and MyD88-deficient mice (A) and TLR3-deficient mice (B) at 12 hpi were compared. The experiments were repeated twice, and representative data are shown.

were inoculated with 10^4 PFU of PV. We suspect that the slight difference between the mortality rates of wild-type and MDA5$^{-/-}$ mice was in the range of experimental fluctuation, and thus, the disruption of MDA5 did not significantly influence the mortality rate. In order to determine if the same is true when mice are infected by other routes, we inoculated wild-type and MDA5$^{-/-}$ mice with PV intracerebrally and compared their mortality rates (Fig. 5G to I). Their mortality rates did not differ significantly. These results suggest that MDA5 does not make a great contribution to the protection of mice, at least after intracerebral and intravenous infections. Taken together, the MDA5-mediated response does not play a dominant role in IFN production, ISG induction, or inhibition of PV replication *in vivo*, unlike the MDA5-mediated effects on EMCV infection.

IFN response in TRIF- and MyD88-deficient mice. Because the experiments with MDA5-deficient mice suggested the existence of other protective mechanisms in PV infection, we investigated the role of TLRs using TRIF- and MyD88-deficient mice. PVR-tg mice were mated with TRIF$^{-/-}$ and/or MyD88$^{-/-}$ mice in the B6 background. Serum IFN-α of mice infected with 10^7 PFU of PV was measured using ELISA at 12 hpi (Fig. 6A). Interestingly, serum IFN production in response to PV infection was abrogated in TRIF$^{-/-}$ mice. Because TRIF acts as an adaptor for TLR3 and TLR4, we tested whether the same phenomenon occurs in TLR3$^{-/-}$ mice. Serum IFN induction was not observed in TLR3-deficient mice (Fig. 6B). These results suggest that the TLR3-mediated pathway is essential for IFN production in response to PV infection.

We next assessed the induction of mRNAs for OAS1a (Fig. 7A) and IRF-7 (Fig. 7B) in various organs using real-time RT-PCR. The induction of OAS1a and IRF-7 was observed in all mice. Although serum IFN production was abrogated in TRIF$^{-/-}$ mice and TRIF$^{-/-}$ MyD88$^{-/-}$ mice (Fig. 6), a significant level of ISG mRNA was induced. However, the induction levels were slightly lower than those in wild-type mice in some cases. The results suggest that the TRIF-mediated pathway contributes to ISG expression mainly through the induction of serum IFNs in response to PV infection and that some other mechanisms may also contribute to ISG expression.

PV replication in nonneural tissues and mortality rates of TRIF- and MyD88-deficient mice. The brain, spinal cord, liver, spleen, and kidney of paralyzed mice were recovered, and viral titers were determined (Fig. 8). PV was recovered from the CNS of TRIF$^{-/-}$, MyD88$^{-/-}$, and TLR3$^{-/-}$ mice, and the titers were not different from those of wild-type mice. However, the viral titers of the liver, spleen, and kidney of TRIF$^{-/-}$ and TLR3$^{-/-}$ mice were significantly higher than those of wild-type mice but lower than those of IFNAR1$^{-/-}$ mice. We then examined the virus replication kinetics in TRIF$^{-/-}$ mice (Fig. 8B). The viral load in the CNS increased in TRIF$^{-/-}$ mice similarly to that in other mice. In accordance to the absence of serum IFN (Fig. 2), the viral loads in the liver, spleen, and kidney of TRIF$^{-/-}$ mice increased, while the viral loads in these organs of wild-type mice decreased. PV antigens were detected in the CNS of all of the knockout mice. In addition, PV antigens were detected in the adipose tissue, pancreas, and kidney of several TRIF$^{-/-}$ and MyD88$^{-/-}$ mice (Table 2). These results suggest that these tissues support viral multiplication in these knockout mice and that the TLR-mediated signaling pathways contribute to the regulation of PV replication in nonneural tissues.

The mortality rates of TRIF$^{-/-}$, MyD88$^{-/-}$, and TLR3$^{-/-}$

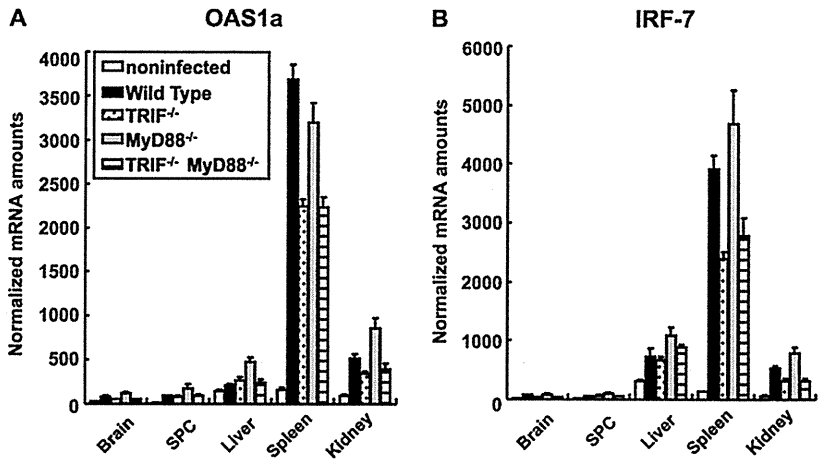

FIG 7 ISG induction in TRIF- and MyD88-deficient mice. Mice (n = 4) were intravenously infected with 10^7 PFU of PV. At 12 hpi, RNA was isolated from the indicated tissues of the infected mice and OAS1a (A) and IRF-7 (B) mRNA levels were determined by quantitative real-time PCR. The experiments were repeated twice, and representative data are shown. SPC, spinal cord.